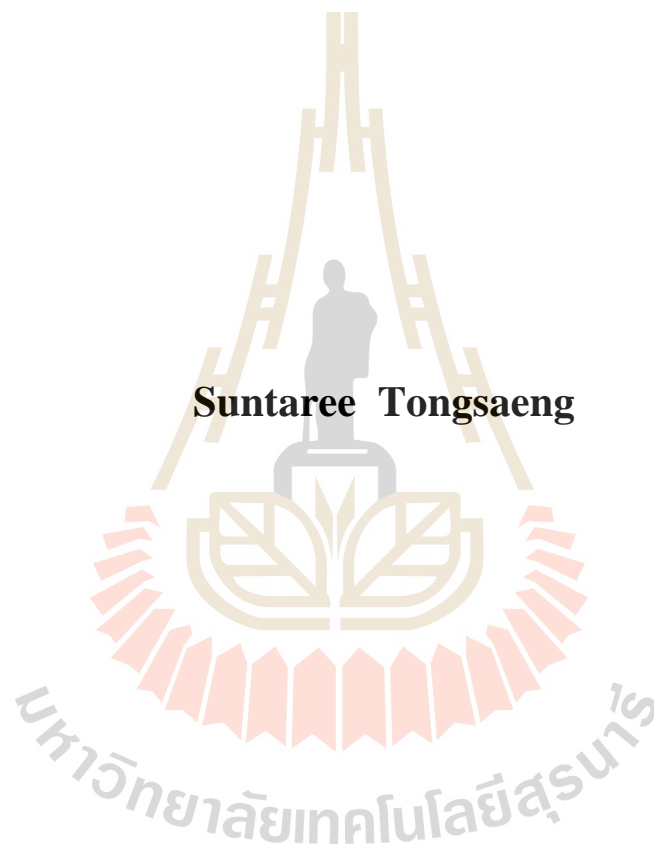


LOCAL STRUCTURE IN Fe-DOPED BaTiO₃
MATERIALS STUDIED BY X-RAY ABSORPTION
SPECTROSCOPY TECHNIQUE



A Thesis Submitted in Partial Fulfillment of the Requirements for the
Degree of Master of Science in Applied Physics
Suranaree University of Technology
Academic Year 2016

การศึกษาโครงสร้างเฉพาะบริเวณในวัสดุแบบเรียบไททานเนตที่เจือด้วยเหล็กโดย
ใช้เทคนิคสเปกโทรสโกปีการดูดกลืนรังสีเอ็กซ์



นางสาวสุนทรี ทองแสง

วิทยานิพนธ์นี้เป็นส่วนหนึ่งของการศึกษาตามหลักสูตรปริญญาวิทยาศาสตรมหาบัณฑิต

สาขาวิชาฟิสิกส์ประยุกต์

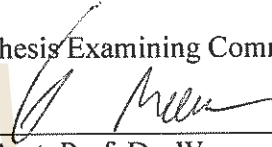
มหาวิทยาลัยเทคโนโลยีสุรนารี

ปีการศึกษา 2559

**LOCAL STRUCTURE IN Fe-DOPED BaTiO₃ MATERIALS
STUDIED BY X-RAY ABSORPTION SPECTROSCOPY
TECHNIQUE**

Suranaree University of Technology has approved this thesis submitted in partial fulfillment of the requirements for a Master's Degree.

Thesis Examining Committee



(Asst. Prof. Dr. Worawat Meevasana)

Chairperson



(Assoc. Prof. Dr. Rattikorn Yimnirun)

Member (Thesis Advisor)



(Dr. Saroj Rujirawat)

Member



(Assoc. Prof. Dr. Prayoon Songsiriritthigul)

Member



(Dr. Pinit Kidkhunthod)

Member



(Prof. Dr. Sukit Limpijumnong)

Vice Rector for Academic Affairs
and Innovation



(Prof. Dr. Santi Maensiri)

Dean of Institute of Science

สุนทรีย ทอแสง : การศึกษาโครงสร้างเฉพาะบริเวณในวัสดุแบเรียมไททานเตที่เจือด้วยเหล็กโดยใช้เทคนิคสเปกโทรสโกปีการดูดกลืนรังสีเอ็กซ์ (LOCAL STRUCTURE IN Fe-DOPED BaTiO₃ MATERIALS STUDIED BY X-RAY ABSORPTION SPECTROSCOPY TECHNIQUE) อาจารย์ที่ปรึกษา : รองศาสตราจารย์ ดร.รัตติก ยัมนิรัญ, 60 หน้า.

วิทยานิพนธ์นี้มุ่งศึกษาความสัมพันธ์ของโครงสร้างเฉพาะบริเวณที่นำไปสู่การเปลี่ยนเฟสของวัสดุ เพื่อให้เข้าใจกระบวนการการเปลี่ยนเฟสได้มากขึ้น ในงานวิจัยนี้วัสดุที่สนใจคือ แบเรียมไททานเตเจือด้วยเหล็ก เพราะมีการนำไปประยุกต์ใช้อย่างแพร่หลาย หาได้ง่ายและไม่เป็นพิษต่อสิ่งแวดล้อม

ในการศึกษาวัสดุแบเรียมไททานเตเจือด้วยเหล็ก ได้ตรวจสอบโครงสร้างผลึกด้วยเทคนิคการเลี้ยวเบนรังสีเอ็กซ์ (XRD) และการดูดกลืนรังสีเอ็กซ์ (XAS) ผลการตรวจสอบจากเทคนิคการเลี้ยวเบนรังสีเอ็กซ์ไม่พบการเปลี่ยนเฟสที่ชัดเจน แต่กลับพบว่าเกิดการเปลี่ยนเฟสของผลึกแบบผสมระหว่างโครงสร้างเตตระโกนอลกับเฮกซะโกนอล โดยการเกิดเฟสโครงสร้างเฮกซะโกนอลเกิดจากการเจือเหล็กและอุณหภูมิของการเผา โดยสัดส่วนของเฟสโครงสร้างเฮกซะโกนอลจะเพิ่มขึ้นตามการเพิ่มของอุณหภูมิของการเผา ส่วนผลการตรวจสอบจากเทคนิคการดูดกลืนรังสีเอ็กซ์ในขอบ K ของเหล็กพบว่าเหล็กเข้าไปแทนที่ไทเทเนียมในแบเรียมไททานเตและพบโครงสร้างเฉพาะบริเวณค้อย ๆ เปลี่ยนรอบอะตอมเหล็ก ซึ่งสอดคล้องกับการคำนวณสเปกตรัมโดยโปรแกรม FEFF 8.2

สาขาวิชาฟิสิกส์
ปีการศึกษา 2559

ลายมือชื่อนักศึกษา สุนทรีย ทอแสง
ลายมือชื่ออาจารย์ที่ปรึกษา รัตติก ยัมนิรัญ

SUNTAREE TONGSAENG : LOCAL STRUCTURE IN Fe-DOPED BaTiO₃
MATERIALS STUDIED BY X-RAY ABSORPTION SPECTROSCOPY
TECHNIQUE. THESIS ADVISOR : ASSOC. PROF. RATTIKORN
YIMNIRUN, Ph.D. 60 PP.

Fe-DOPED BaTiO₃/ LOCAL STRUCTURE

This thesis was aimed to study the relationship of local structure and a change in the structure of the crystalline phase to understand the phase transformation better. The material of interest was iron-doped barium titanate because it has been used widely, easy to find and non-toxic to environment.

In Fe-doped BaTiO₃ (Fe-BTO) material, the phase information was investigated by X-ray Diffraction (XRD) and X-ray Absorption Spectroscopy (XAS). The results of X-ray diffraction technique did not clearly show the phase transition in Fe-BTO. However, changes in the structure of the crystalline phase with a mixture of tetragonal and hexagonal structures were observed. The formation of hexagonal phase was a result of Fe dopant and the sintering temperature. The portion of the hexagonal phase was increased with increasing the sintering temperature. The Fe K-edge X-ray Absorption Near Edge Structure (XANES) spectra showed that Fe atoms substituted in Ti sites in BaTiO₃ and local structure gradually changed around Fe atoms. This was consistent with the calculated spectrum by FEFF8.2 application.

School of Physics

Academic Year 2016

Student's Signature Suntaree Tongsaeng

Advisor's Signature Rattikorn Yimnirun

ACKNOWLEDGEMENTS

I am very grateful to my advisor Assoc. Prof. Dr. Rattikorn Yimnirun for his great advisory, kind patience, guidance, and inspiring me the way to be a good researcher. He has friendship and kind support for me. I would like to thank my co-advisor Dr. Saroj Rujirawat and I would like to thank Asst. Prof. Dr. Worawat Meevasana, Assoc. Prof. Dr. Prayoon Songsiriritthgul, and Dr. Pinit Kidkhunthod for contributing as my advisory committee members.

I would like to acknowledge all staff members of the Center for Scientific and Technological Equipment, Suranaree University of Technology and the Synchrotron Light Research Institute (Public Organization), Thailand for their helps in operating equipments during specimen characterizations. I also would like to thank Dr. Atipong Bootchanont and Dr. Jaru Jutimoosik for their helps. Importantly, this work would not be completed without supports and help from the faculties of the School of Physics, Suranaree University of Technology.

Finally, I would like to express appreciation to my parents and brother for great support, encouragement and good advices to me throughout my studies.

Suntaree Tongsaeng

CONTENTS

	Page
ABSTRACT IN THAI.....	I
ABSTRACT IN ENGLISH	II
ACKNOWLEDGEMENTS.....	III
CONTENTS.....	IV
LIST OF TABLES	VII
LIST OF FIGURES	VIII
LIST OF ABBREVIATIONS.....	XI
CHAPTER	
I INTRODUCTION.....	1
1.1 Background.....	1
1.2 Research objectives.....	2
1.3 Scope and limitation of the study.....	2
II LITERATURE REVIEWS	3
2.1 Barium titanate.....	3
2.2 Fe-doped barium titanate	4
2.3 X-ray diffraction (XRD)	5
2.4 X-ray absorption spectroscopy (XAS)	8
2.4.1 X-ray absorption near edge structure (XANES)	10
2.4.2 Extended x-ray absorption fine structure (EXAFS)	11

CONTENTS (Continued)

	Page
2.5 XRD and XAS studies in BTO and Fe-BTO	14
III MATERIALS AND METHODS	18
3.1 Solid state reaction synthesis	18
3.1.1 BaTiO ₃ and Ba(Ti,Fe)O ₃	18
3.2 X ray diffraction setup	20
3.3 X-ray absorption spectroscopy setup	23
3.3.1 X-ray absorption spectroscopy experimental setup	23
3.3.2 X-ray absorption spectrum calculation	28
3.4 Experimental details	30
IV RESULTS AND DISCUSSION	31
4.1 X-ray diffraction (XRD)	31
4.2 XANES results	35
4.2.1 Identification of Fe site in BaTiO ₃	35
4.2.2 XANES studies of Ti K pre-edge	36
4.2.3 XANES studies of phase transition	37
4.3 EXAFS results	41
V CONCLUSIONS	44
REFERENCES	45
CURRICULUM VITAE	49

LIST OF TABLES

Table	Page
4.1 The lattice parameters and the ratio of BaTiO_3	32
4.2 The lattice parameters and the ratio of $\text{BaFe}_{0.01}\text{Ti}_{0.99}\text{O}_3$	32



LIST OF FIGURES

Figure	Page
2.1	Crystal structure of cubic perovskite BaTiO ₃ 3
2.2	The phase transition of BaTiO ₃ 4
2.3	Crystal structure of cubic perovskite BaFeO ₃ 5
2.4	The X-ray diffraction beam path..... 6
2.5	Schematic view of x-ray absorption measurement in transmission mode.....8
2.6	Diagram of the electron transition in inner shell 9
2.7	Normalized XAS data 10
2.8	The EXAFS mechanism of photo electron scattering..... 12
2.9	(a) X-ray diffraction patterns of BaTi _{1-x} Fe _x O ₃ powder samples treated at different annealing temperatures. The peaks of tetragonal (top) and hexagonal (bottom) BaTiO ₃ are labeled with Miller indices (hkl). (b) Magnification of diffraction peaks in the 2θ interval 30°–34°, which shows the effect of annealing temperature on the phase evolution of Fe-doped BaTiO ₃ 15
2.10	Normalized Fe K-edge XANES spectra measured on the 10% Fe-doped 6H-BaTiO ₃ samples after the different heat treatments and reference compounds[Fe(III) ₂ O ₃ , NdFe(III)O ₃ , and Fe(II)SO ₄] with known Fe valance state. Two vertical lines are plotted at the position of the Fe(II) K-edge (7121 eV) and Fe(III) Kedge (7125.7 eV) for comparison of the Fe K-edge positions16

LIST OF FIGURES (Continued)

Figure	Page	
2.11	Normalized Ti K-edge XANES spectra measured on 10% Fe-doped 6H–BaTiO ₃ powder samples, treated at different annealing temperatures (1250°C and 1500°C), and undoped BaTiO ₃ with tetragonal (space group P4mm) crystal structure as a standard for Ti ⁴⁺	17
3.1	Flow chart of the synthesis of Ba(Ti _{0.99} Fe _{0.01})O ₃ powders	19
3.2	Flow chart of the synthesis of Ba(Ti _{0.99} Fe _{0.01})O ₃ ceramics	20
3.3	Schematic illustration of θ -2 θ x-ray diffraction experiment.	22
3.4	Schematic representation of X-ray diffractometer D5005	22
3.5	The three modes of XAS measurement (a) transmission mode, (b) fluorescence mode and (c) electron yield.	24
3.6	Schematic illustration of the experimental setup of transmission-mode X-ray absorption spectroscopy	25
3.7	XAS experimental set up at the Siam Photon Laboratory, Synchrotron Light Research Institute	25
3.8	The excited state (a) x-ray fluorescence and (b) the Auger effect	27
3.9	Detail of an atoms.inp input file to generate “feff.inp” for FEFF calculation.	28
4.0	Detail of a “feff.inp” input file of MgO with Mg as center atom for FEFF calculation	29
4.1	X-ray diffraction patterns of BaTiO ₃	32
4.2	X-ray diffraction patterns of Ba(Fe _{0.01} Ti _{0.99})O ₃	32

LIST OF FIGURES (Continued)

Figure	Page
4.3	Model crystals structure of BaTiO ₃ . b–c Schematic illustrations of Fe on Ti site, Fe on Ba site, respectively 35
4.4	Fe K-edge XANES spectra of BaTi _{0.9} Fe _{0.1} O ₃ And calculation of Fe site for Fe on Ti site (Fe _{Ti} -pink line), Fe on Ba site (Fe _{Ba} -gold line) 36
4.5	Normalized Fe K-edge XANES spectra measured on the Fe-BTO samples and reference compounds (Fe ₂ O ₃ , FeO, and Fe foil) with known Fe valance state 37
4.6	Normalized X-ray absorption Ti K pre-edge spectra of BaFe _{0.01} Ti _{0.99} O ₃ 38
4.7	Normalized X-ray absorption Ti K-edge spectra of Ba(Fe _{0.01} Ti _{0.99})O ₃ 40
4.8	Comparison of Normalized X-ray absorption Ti K-edge spectra of Ba(Fe _x Ti _{1-x})O ₃ with simulated features of Ti K-edge XANES spectra of Ba(Fe,Ti)O ₃ tetragonal (pinkline) and hexagonal (gold line) 41
4.9	The Normalized Fe K-edge EXAFS spectra of Ba(Ti,Fe)O ₃ 42
4.10	The EXAFS Fourier transform in k-space of Ba(Ti,Fe)O ₃ 43
4.11	The EXAFS models in k-space of Ba(Ti,Fe)O ₃ 43

LIST OF ABBREVIATIONS

°C	degree Celcius
T	Temperature
TC	Curie temperature
BL5.2	Beamline 5.2
BT	Barium Titanate
BFT	Fe doped Barium Titanate
XRD	X-ray Diffraction
XAS	X-ray Absorption Spectroscopy
XANES	X-ray Absorption Near Edge Structure
EXAFS	Extended X-ray Absorption Fine Structure

CHAPTER I

INTRODUCTION

1.1 Background

Over the years since the discovery of ferroelectricity materials in 1921 and its subsequent extension into the realm of polycrystalline ceramics (barium titanate, BaTiO_3) during the early to mid-1940s (Gene H. Haertling (1999)), barium titanate (BaTiO_3) exhibits ferroelectric behavior with high dielectric constant, large pyroelectric coefficient and low cost of manufacturing. It is also an environmental friendly material to replace the disadvantages of lead-based materials with volatility and toxicity.

The chemical composition of BaTiO_3 is highly stable, making it easier to sintered with certainty of the chemical composition. However, the use of such materials often have to put up with certain additives, to change and improve the basic properties. The ferroelectric properties of barium titanate (BaTiO_3) can be controlled by doping with different elements. Material of each type has a different properties. Interestingly, an increase of Fe substitution on the site Ti in BaTiO_3 crystal material can change structure and exhibit relaxor ferroelectric behavior. The addition of Fe causes a phase change from tetragonal to hexagonal. In this study, we aim to examine the difference of local structure in BaTiO_3 and Fe-BTO materials by using the X-ray Absorption Spectroscopy (XAS) technique to study their local structure.

1.2 Research objectives

- a) To synthesize BaTiO_3 and $\text{Ba}(\text{Ti}_{1-x}\text{Fe}_x)\text{O}_3$ powders and ceramics by the solid state reaction method.
- b) To study the global structure and local structure of BaTiO_3 and $\text{Ba}(\text{Ti}_{1-x}\text{Fe}_x)\text{O}_3$ by XRD and XAS, respectively.
- c) To study structural phase transition and of BaTiO_3 and $\text{Ba}(\text{Ti}_{1-x}\text{Fe}_x)\text{O}_3$.

1.3 Scope and limitation of the study

This study is intended to synthesize BaTiO_3 and $\text{Ba}(\text{Ti}_{1-x}\text{Fe}_x)\text{O}_3$ materials by the solid state reaction method. The standard XRD will be used as an aid in determining the global structure of the prepared materials. The local structure of BaTiO_3 and $\text{Ba}(\text{Ti}_{1-x}\text{Fe}_x)\text{O}_3$ materials will be characterized by XAS. FEFF 8.2 code (Chandarak *et al.*, 2012) will be used to simulate XANES spectra of BaTiO_3 and $\text{Ba}(\text{Ti}_{1-x}\text{Fe}_x)\text{O}_3$ to compare with experiment.

CHAPTER II

LITERATURE REVIEWS

2.1 Barium titanate

Barium titanate is another type of ABO_3 perovskite and dielectric material with the chemical formula $BaTiO_3$. The structure of $BaTiO_3$ is a tetragonal perovskite structure. When the temperature is higher than the Curie temperature, barium titanate is a cubic structure, consisting of octahedral TiO_6 centres that define a cube with Ti vertices and Ti-O-Ti edges and Ba^{2+} is located at the center of the cube, as shown in Figure 2.1

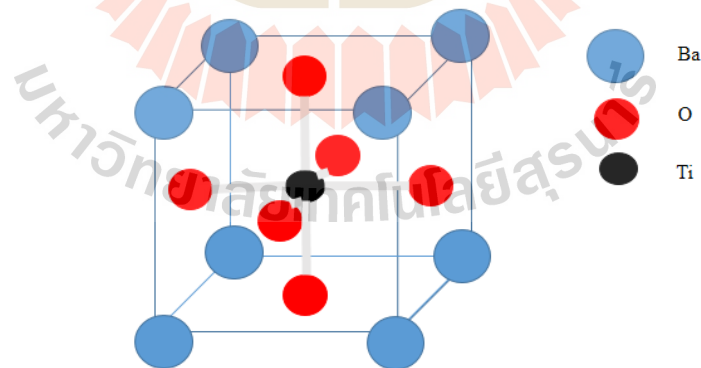


Figure 2.1 Crystal structure of cubic perovskite $BaTiO_3$.

Barium titanate can exhibit phase transition with various temperatures (T), as shown in Figure 2.2. At $T \leq -90^\circ\text{C}$, the structure of $BaTiO_3$ is rhombohedral,

between -90°C to 5°C , the rhombohedral structure change to orthorhombic. Above 5°C , the orthorhombic cell changes to tetragonal, at Curie temperature (T_C) about 120°C , the tetragonal changes structure to cubic cell and the cubic structure changes to hexagonal cell at temperatures above 1450°C (Maiti *et al.*, 2008).

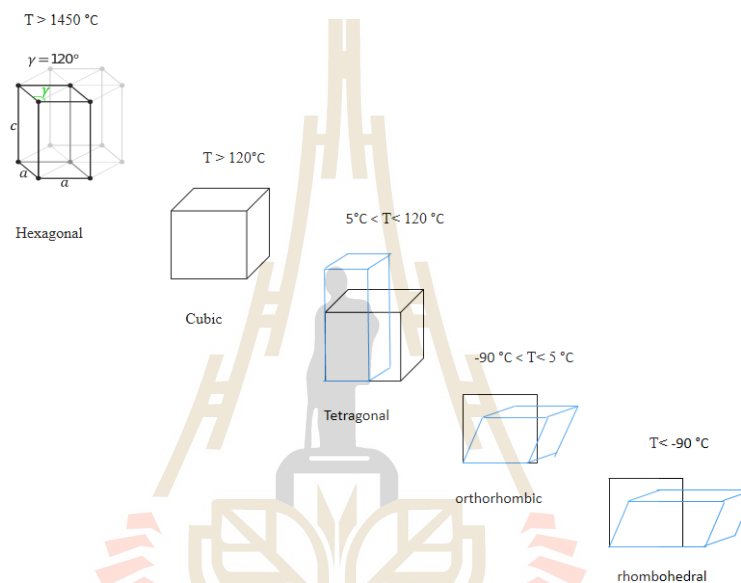


Figure 2.2 The phase transition of BaTiO₃.

2.2 Fe-doped Barium titanate

Barium iron titanate is a lead-free ferroelectric with the chemical formula Ba(Ti,Fe)O₃. BaFeO₃ is known to exhibit paraelectric behavior because of its crystal symmetry with no spontaneous polarization (Figure 2.3). When Ti suitably substitutes for Fe, the ferroelectric behavior is observed.

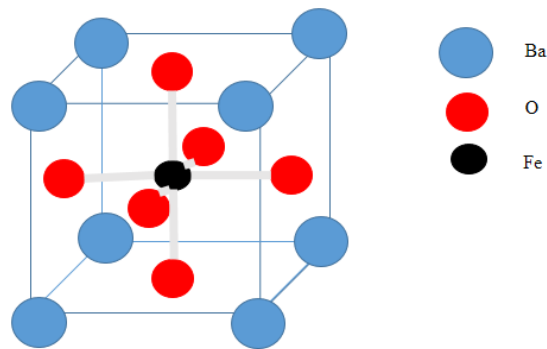


Figure 2.3 Crystal structure of cubic perovskite BaFeO₃.

Barium iron titanate is known to exhibit relaxor behavior in bulk materials with increasing Fe content. Substitution of Fe³⁺ with Ti⁴⁺ exhibits several interesting features in the dielectric behavior of BaTiO₃. It has been reported that with the incorporation of Fe in BaTiO₃, the tetragonal to hexagonal phase transition temperatures corresponding to pure BaTiO₃ increases (X.K.Wei *et al.*, 2011).

2.3 X-ray Diffraction (XRD)

X-ray powder diffraction (XRD) is a rapid analytical technique primarily used for phase identification of a crystalline material and can provide information on unit cell dimensions. The analyzed material is finely ground, homogenized, and average bulk composition is determined. However, X-ray diffraction cannot determine amorphous materials because fundamental treatment of X-ray diffraction by crystals is done by considering the interaction of an X-ray plane wave with the electrons of the crystal materials. While, the wave nature of X-ray incident on plan of crystal that occur reflection and the path difference of two plan equal amount of wavelength of

the X-ray beam, as shown in Figure 2.4. The diffracted beams from atoms in successive planes cancel unless they are in phase, and the condition for this is given by the Bragg relationship;

$$2d \sin \theta = n\lambda, \quad (2.1)$$

where d is the distance between adjacent planes of atoms,

θ is the angle of incidence of the x-ray beam,

n is the order of the diffracted beam,

and λ represents the wavelength of the incident x-ray beam.

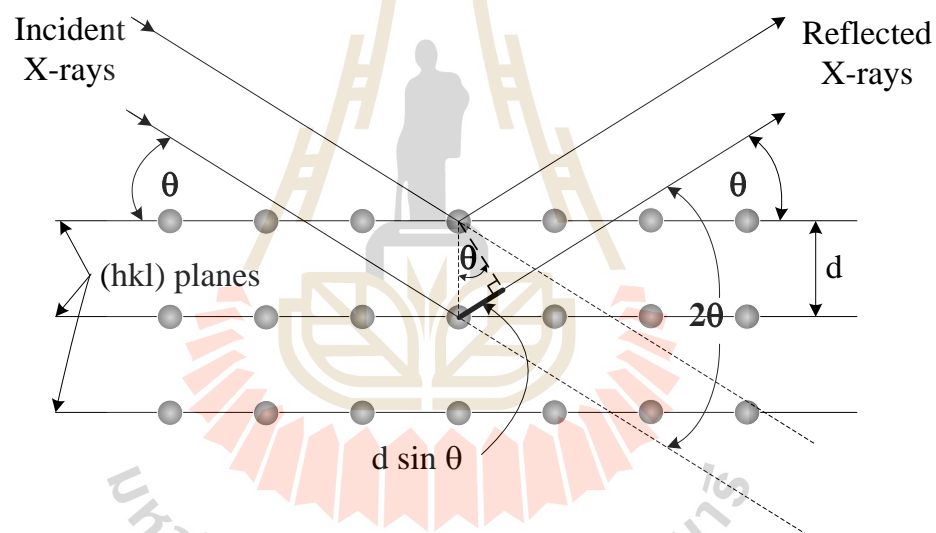


Figure 2.4 The X-ray diffraction beam path. (Jutimoosik, 2010).

The Miller indices ($h k l$) can be calculated from Bragg's law:

$$2d_{hkl} \sin \theta = n\lambda. \quad (2.2)$$

In the cubic systems, the plane spacing is connected to the lattice parameter and the Miller indices by the following relation:

$$d_{hkl} = \frac{a}{\sqrt{h^2 + k^2 + l^2}}. \quad (2.3)$$

Combining equation (2.2) and (2.3), we get

$$a_{hkl} = \frac{n\lambda\sqrt{h^2 + k^2 + l^2}}{2\sin\theta}. \quad (2.4)$$

Considering the non cubic systems such as hexagonal system, the Miller indices can be calculated by using the lattice parameter from Bravais lattice:

$$\frac{1}{d^2} = \frac{4}{3} \left(\frac{h^2 + hk + k^2}{a^2} \right) + \frac{l^2}{c^2}. \quad (2.5)$$

Recall Bragg's law:

$$2d \sin\theta = \lambda, \quad (2.6)$$

$$4d^2 \sin^2\theta = \lambda^2, \quad (2.7)$$

$$\frac{1}{d^2} = \frac{4 \sin^2\theta}{\lambda^2}. \quad (2.8)$$

Combining equation (2.5) and (2.8), we obtain

$$\frac{1}{d^2} = \frac{4}{3} \left(\frac{h^2 + hk + k^2}{a^2} \right) + \frac{l^2}{c^2} = \frac{4 \sin^2\theta}{\lambda^2}. \quad (2.9)$$

We can rearrange equation (2.9) in term of $\sin^2\theta$ as,

$$\sin^2\theta = \left(\frac{\lambda^2}{4a^2} \right) * \left[\frac{4}{3} (h^2 + hk + k^2) + \frac{l^2}{(c/a)^2} \right], \quad (2.10)$$

where a and c/a are constants for a given diffraction pattern.

2.4 X-ray absorption spectroscopy (XAS)

X-ray Absorption Spectroscopy is the powerful technique for identifying local structure site of element, formal oxidation state, coordination number and used to examine the electronic structure of materials. The XAS experiment is normally carried out at the synchrotron radiation facility, which can be modified and selected the energy of X -ray photon (Koningsberger and Prins, 1988).

The X-ray absorption coefficient is determined from the decay in the X-ray intensity I with the length of a sample x by the relationship,

$$I = I_0 e^{-\mu x}, \quad (2.11)$$

where I_0 is the intensity of the incoming x-ray beam,

I is the intensity of the beam after pass through the sample,

x is the thickness of the sample,

and μ is the definition of absorption coefficient, as shown in Figure 2.5.

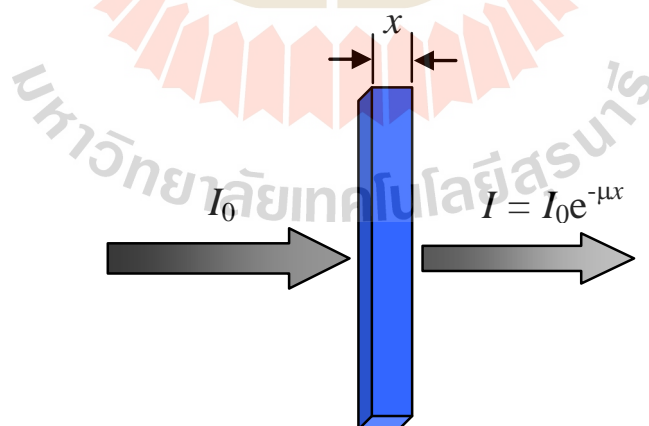


Figure 2.5 Schematic view of X-ray absorption measurement in transmission mode

(Jutimoosik, 2010).

In the X-ray absorption process, a photon is absorbed by the atom, giving rise to the transition of the electrons from the inner shells: K, L or M shell to empty state above the Fermi level. The core hole, empty state, will be created in the inner shell, and the energy level of the shell is used to identify the type of absorption edge as shown in Figure 2.6. For example, K-edge refers to transition that excited electron from 1s shell to unoccupied states. The x-ray photon energy has to be greater than the difference of energy between unoccupied states and K shell state. The energy of the absorption edges are specific characteristic to elements, making X-ray absorption an element-selective technique.

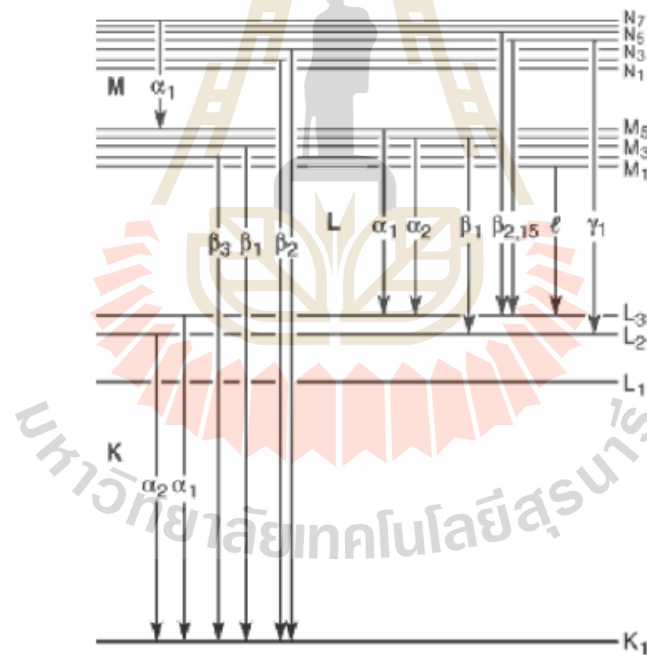


Figure 2.6 Diagram of the electron transition in inner shell (Thompson *et al.*, 2001).

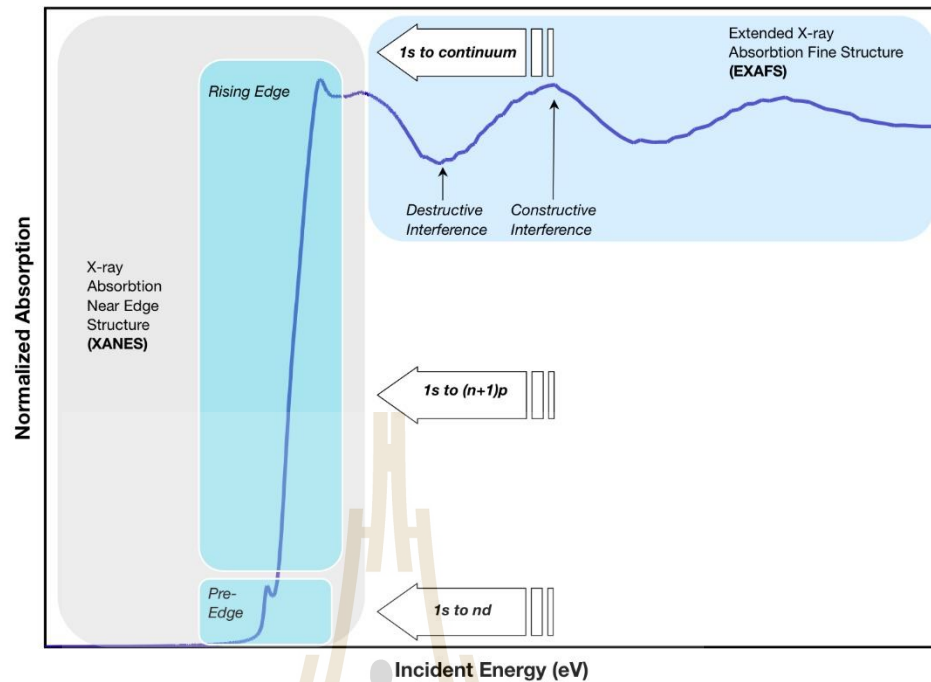


Figure 2.7 Normalized Absorption XAS data.

There are three main regions found on a spectrum generated by XAS data (1) Pre-Edge (2) X-ray Absorption Near Edge Structure (XANES), which ends about 80-100 eV above the edge and (3) Extended X-ray Absorption Fine Structure (EXAFS), which starts about 50 eV above the edge and extends at up to 1000 eV, as shown in Figure 2.7.

2.4.1 X-ray absorption near edge structure (XANES)

X-ray absorption near edge structure, or XANES, contains the information about the chemical state of the element, including the oxidation state, and the local geometry of the absorbing atom.

This region of the absorption spectrum is dominated by multiple scattering of low energy of photoelectron. In addition, there are normally strong features due to transitions to empty bonding and anti-bonding orbitals in molecular systems, or to

atomic-like or unoccupied density of state in solid state systems. The combination of these influence mean that XANES is sensitive to the local electronic structure of the absorbing species and the coordination geometry. XANES has most often been used in a fingerprint fashion, with spectra compared to standards to determine the quantity of interest such as the oxidation state of the absorbing element.

The absorption coefficient in equation (2.11) is proportional to the transition rate as given by Fermi's Golden Rule; described by

$$\tilde{\mu}(E) \propto \sum_f |\langle f | \hat{\epsilon} \cdot \vec{r} | i \rangle|^2 \delta(E_i - E_f + \hbar\omega), \quad (2.12)$$

where $|i\rangle$ is the initial core *ket* state vector, $\langle f|$ is the final *bra* state vector of the excited electron, E is the energy of absorbed x-ray photon, E_i is the energy of initial state, E_f is the energy of final state, $\hbar\omega$ is the energy of x-ray photon energy, $\hat{\epsilon}$ is the x-ray polarization vector and $\tilde{\mu}(E)$ is absorption coefficient with ignoring of core hole life time and experimental resolution (Ankudinov *et al.*, 1998). By considering Eq. further with the additional effects of core-hole life time and experimental resolution, the XANES spectra can be calculated as described later in section 3.3.2.

2.4.2 Extended x-ray absorption fine structure (EXAFS)

The extended X-ray absorption fine structure is the oscillating part of the X-ray absorption spectrum that extends to about 1,000 eV above the absorption edge. Analyses of the EXAFS spectrum provide information about the number, species and inter-atomic distances of the neighbors from the absorption atom. EXAFS is a result of the adjustment of the photoelectron final state due to scattering by the surrounding atoms. The final state photoelectron is changed to first order by a single scattering from each surrounding atom. According to quantum theory this photoelectron can be

visualized as a wave emitted from the absorber with wavelength λ is given by the de Broglie relation. In EXAFS region, the momentum of the photoelectron p can be defined by the free electron relation

$$\frac{p^2}{2m} = h\nu - E_0, \quad (2.13)$$

where $h\nu$ is the energy of frequency ν photon, E_0 is the bonding energy of the photoelectron and m is mass of the excited electron.

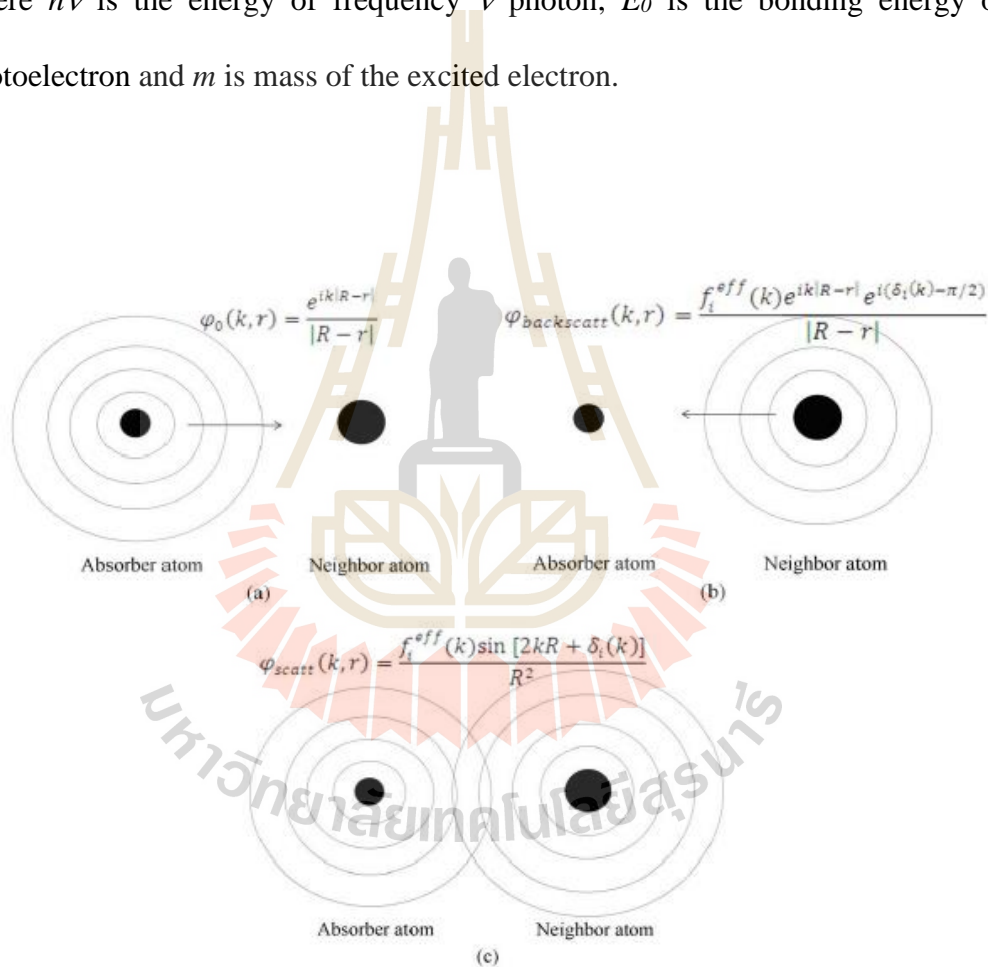


Figure 2.8 The EXAFS mechanism of photo electron scattering.

The oscillatory part of the X-ray absorption above a given absorption edge, EXAFS function can be defined by

$$\chi(E) = \frac{[\mu(E) - \mu_0(E)]}{\Delta\mu_0}, \quad (2.14)$$

where $\mu(E)$ is the X-ray absorption coefficient, $\mu_0(E)$ is smooth atomic background absorption coefficient.

Furthermore, in the EXAFS analysis $\chi(E)$ could be transformed from E space to k space by the relations $k = \sqrt{2m(E - E_0)/\hbar^2}$. Then the function can be converted from $\chi(E)$ to $\chi(k)$ for general purpose. In theoretical procedure, the $\chi(k)$ can be described by (Wilson *et al.*, 2000)

$$\chi(k) = \sum_j \frac{S_0^2 N_j}{k R_j^2} |f_j(k, \pi)| \sin[2kR_j + \varphi_j(k)] e^{-2\sigma_j^2 k^2} e^{-2R_j/\lambda(k)}, \quad (2.15)$$

where N_j is the number of neighbor in j^{th} shell of surrounding atoms, k is photoelectron wave vector, f_j is the scattering amplitude, $S_0^2(k)$ is the amplitude reduction term due to many-body effect, R_j is radial distance from absorbing atom to j shell, $\lambda(k)$ is electron mean free path, σ_j is the Debye-Waller factor and $\varphi(k)$ accounts for the total phase shift of the curve wave scattering amplitude along the scattering trajectory.

The distance between core atom and backscattering atoms or the path-length change the phase contrasting with the wavelength of photoelectron. Furthermore, different types of surrounding atoms vary the backscattering intensity as a function of photoelectron energy. It is accepted that, by the careful analysis of the EXAFS structure, one can receive significance structural parameters surrounding the center atom.

2.5 XRD and XAS studies in BTO and Fe-BTO

The effect of annealing temperature on magnetic properties of 2% and 10% Fe-doped BaTiO₃ was investigated (Mikulska *et al.*, 2014). To understand the possible structural differences between samples treated at different annealing temperatures, and to correlate them with the magnetic properties, several characterization techniques, such as X-ray diffraction and X-ray absorption spectroscopic methods (XANES and EXAFS) were employed. It was found that the 2% Fe-doped BaTiO₃ pseudocubic perovskite is paramagnetic, regardless of the heat-treatment conditions. Initially paramagnetic 10% Fe-doped 6H-BaTiO₃, treated at 1250°C, became ferromagnetic after additional annealing at higher temperature. The cation ordering processes in the 6H-BaTiO₃ that occurred during the high-temperature annealing. The ferromagnetism that was induced in this stage was most probably associated with the observed diffusion processes but its extrinsic character still cannot be fully disregarded.

The crystal structures were analyzed by XRD. 2% Fe-doped BaTiO₃ sample treated at 1200°C has tetragonal crystal structure (space group P4mm) with possible traces of hexagonal phase (space group P63/mmc). The XRD pattern of 2% Fe-doped BaTiO₃ additionally annealed at 1400°C for 5 h indicates the presence of mixture of hexagonal and tetragonal phases. In addition to prevailing 6H phase, the sample with 10% of Fe treated at 1250°C contains minor amount of the tetragonal perovskite phase. The sample additionally annealed at 1500°C shows a single-phase composition with only hexagonal phase.

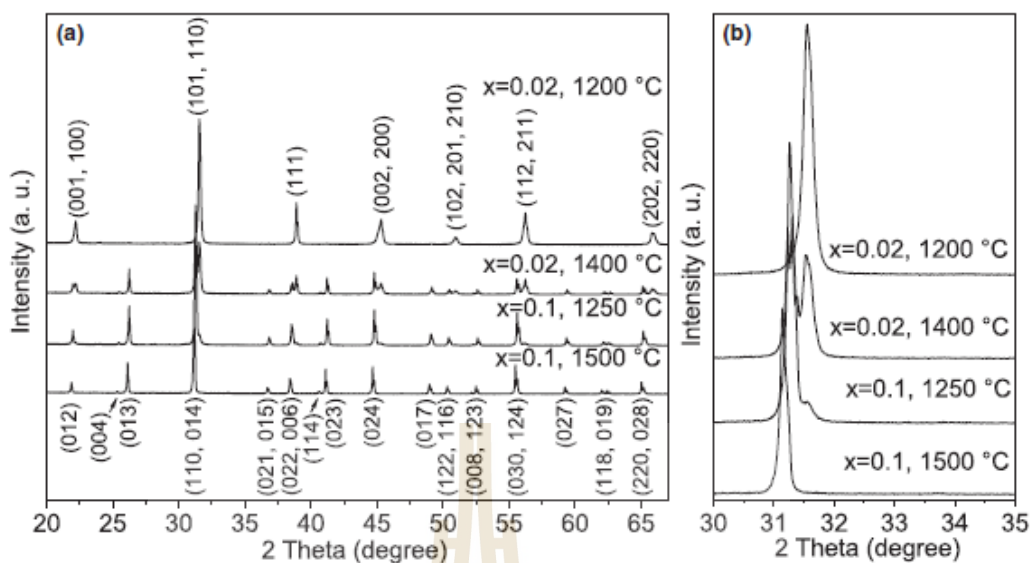


Figure 2.9 (a) X-ray diffraction patterns of $\text{BaTi}_{1-x}\text{Fe}_x\text{O}_3$ powder samples treated at different annealing temperatures. The peaks of tetragonal (top) and hexagonal (bottom) BaTiO_3 are labeled with Miller indices (hkl). (b) Magnification of diffraction peaks in the 2θ interval 30° – 34° , which shows the effect of annealing temperature on the phase evolution of Fe doped BaTiO_3 (Mikulska *et al.*, 2014).

The detailed analysis of Fe valence state and local structure around Fe cations in the crystal structure was performed by Fe K-edge XANES and EXAFS. To verify the possible changes in the valence state of the Fe cations in the 10% Fe-doped 6H- BaTiO_3 samples, Fe K-edge XANES spectra were analyzed. A decrease in the oxidation state of the absorbing atom shifts the energy position of the absorption edge to the lower energies. A shift of about 4.5 eV is observed between Fe^{3+} and Fe^{2+} in reference compounds with well-established Fe valence states (Fe^{3+} in Fe_2O_3 and NdFeO_3 , and Fe^{2+} in FeSO_4).

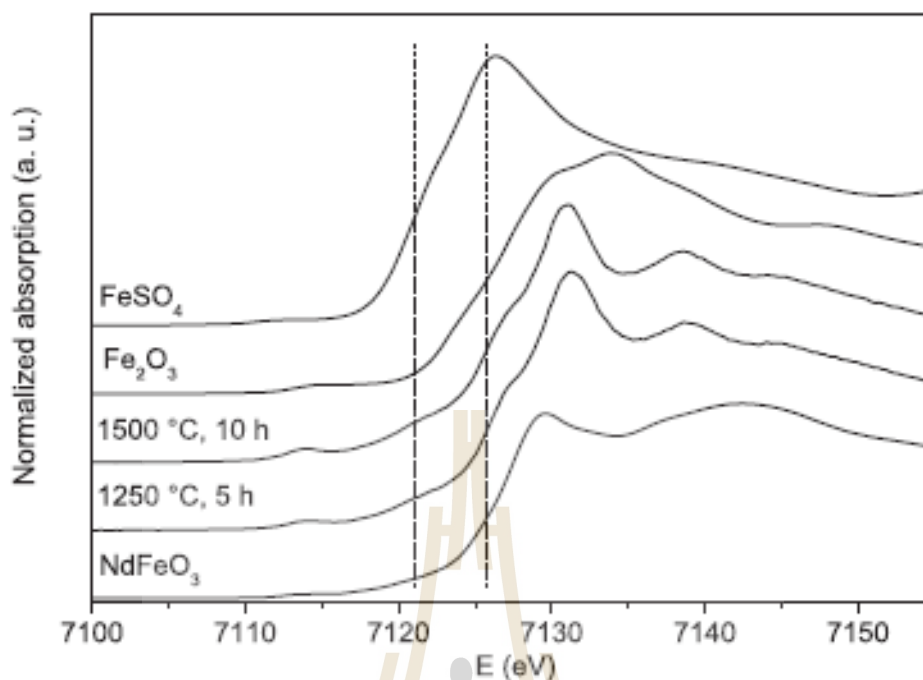


Figure 2.10 Normalized Fe K-edge XANES spectra measured on the 10% Fe-doped 6H-BaTiO₃ samples after the different heat treatments and reference compounds [Fe(III)₂O₃, NdFe(III)O₃, and Fe(II)SO₄] with known Fe valence state. Two vertical lines are plotted at the position of the Fe(II) K-edge (7121 eV) and Fe(III) Kedge (7125.7 eV) for comparison of the Fe K-edge positions (Mikulska *et al.*, 2014).

A comparison of Ti K-edge XANES spectra of the different Fe-doped 6H-BaTiO₃ samples shows that the spectra are identical. The Ti K-edge spectrum of the reference undoped tetragonal perovskite BaTiO₃, which is a well established reference for Ti⁴⁺ valence state, slightly differs in the shape of the edge and preedge features, compared with spectra of the two samples, due to the difference in the crystal structures. However, the energy position of the Ti K-edge in the samples coincides

well with that in undoped perovskite BaTiO_3 , so it can be concluded that all titanium in the 6H- BaTiO_3 samples is in tetravalent state.

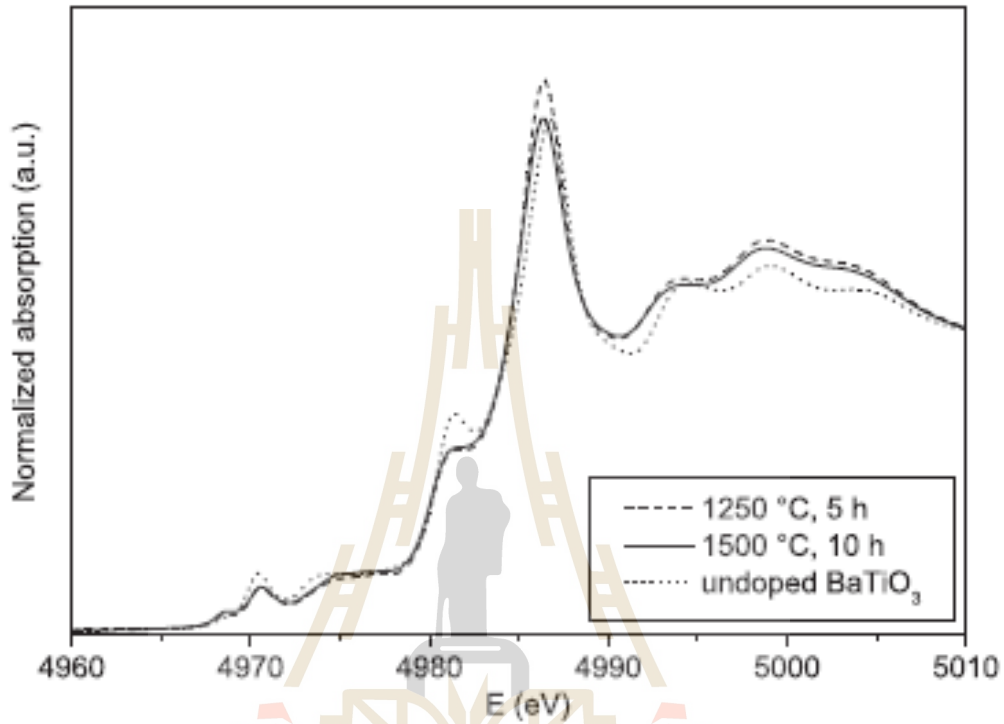


Figure 2.11 Normalized Ti K-edge XANES spectra measured on 10% Fe-doped 6H- BaTiO_3 powder samples, treated at different annealing temperatures (1250°C and 1500°C), and undoped BaTiO_3 with tetragonal (space group $P4mm$) crystal structure as a standard for Ti^{4+} . (Mikulska *et al.*, 2014).

CHAPTER III

MATERIALS AND METHODS

3.1 Solid state reaction synthesis

3.1.1 BaTiO₃ and Ba(Ti,Fe)O₃

In these two systems, the solid state reaction method was used to synthesize the materials via chemical reactions, shown as



The mixing between starting oxide materials by the zirconium ball milling in ethanol solution. After that, the mixed powders were dried by hot plate at temperature about 100°C. Finally, the yield of powders was calcined in furnace at high temperature suitable for each material.

Ba(Ti,Fe)O₃ powders were prepared via methods of the solid state reaction. The starting materials BaCO₃ (99.98%) TiO₂ (99.98%), and Fe₂O₃ (99.98%) were weighed according to the *stoichiometric* composition BaTiO₃. For Ba(Ti_{1-x}Fe_x)O₃ with $x = 0,0.01$ the raw materials were weighed and ball milled in ethanol for 24 h. After drying, the powders were calcined at 1250°C for 2 h. The procedures are shown in Figure 3.1.

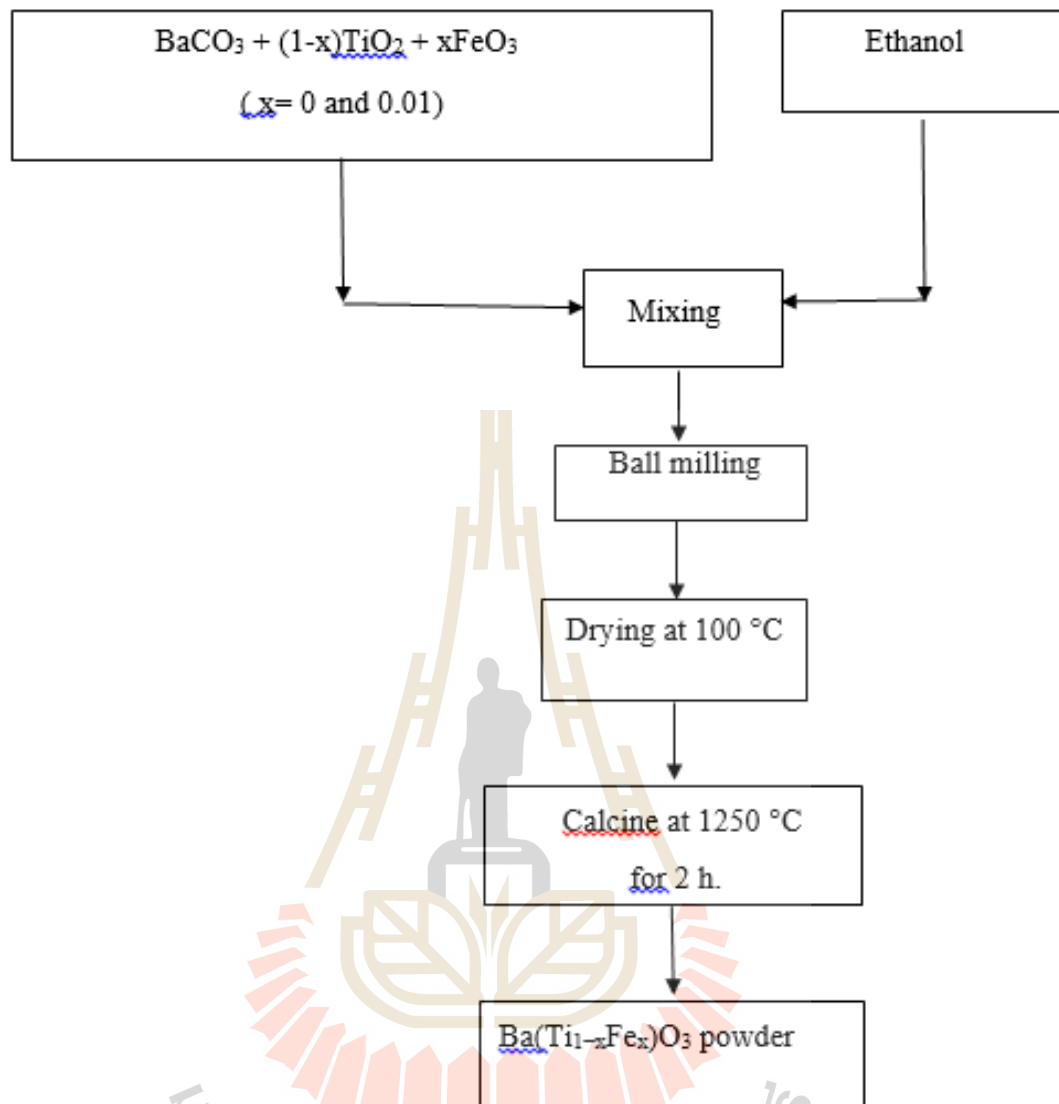


Figure 3.1 Flow chart of the synthesis of $\text{Ba}(\text{Ti}_{1-x}\text{Fe}_x)\text{O}_3$ powders.

After that, the $\text{Ba}(\text{Ti},\text{Fe})\text{O}_3$ powders were mixed with polyvinyl alcohol and made to bulk ceramics by pressed in disks holder about 1.5 mPa, diameter about 10 mm and thickness about 1 mm. The pellets were burned the polyvinyl alcohol at 500°C for 2 h and sintered at $1400\text{--}1500^\circ\text{C}$ for 2 h. The synthesis flowchart is shown as Figure 3.2.

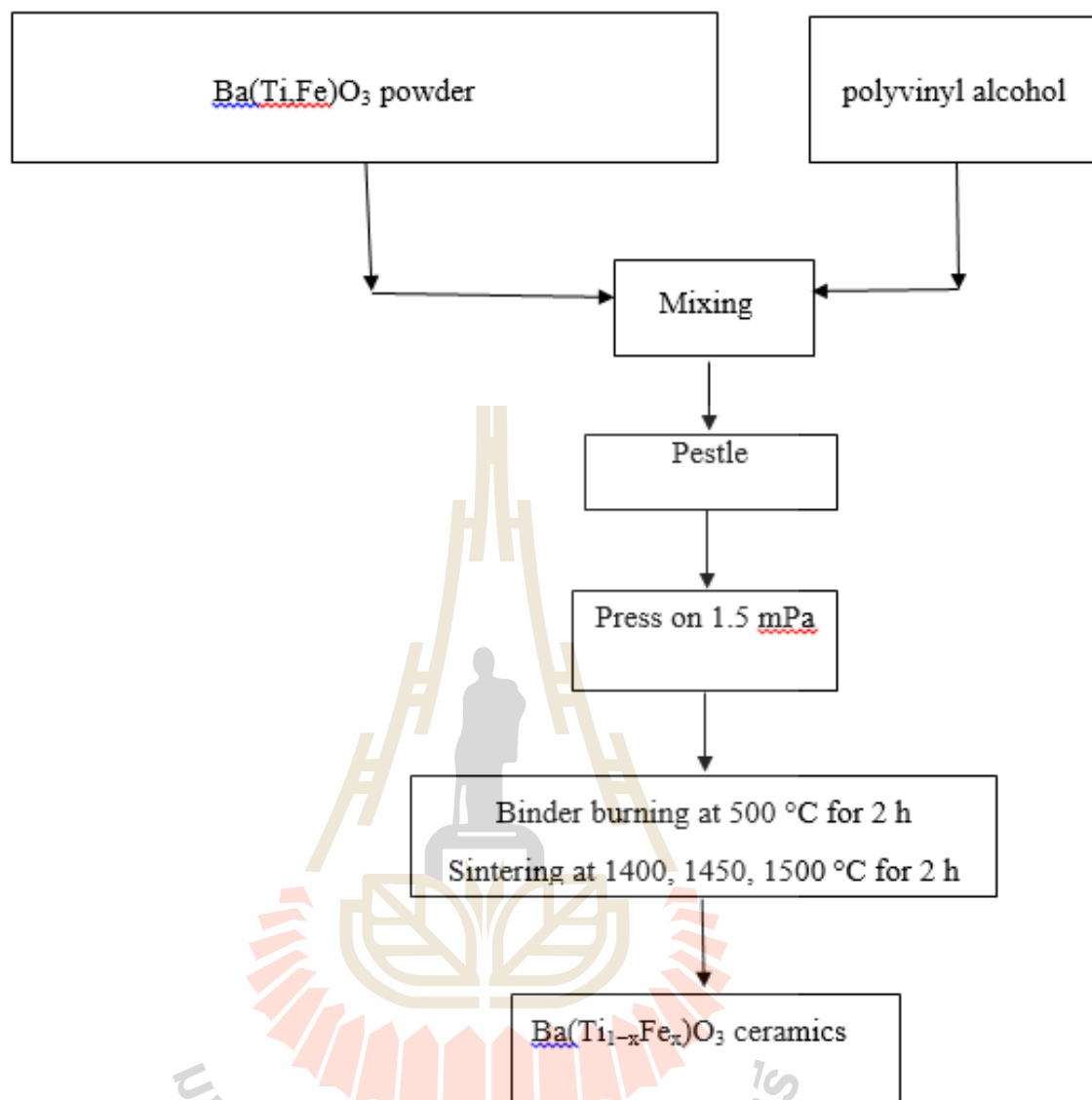


Figure 3.2 Flow chart of the synthesis of $\text{Ba}(\text{Ti}_{1-x}\text{Fe}_x)\text{O}_3$ ceramics.

3.2 X-ray diffraction setup

The Bragg condition can be proper for each planes of crystal. The half wavelength of the x-ray is smaller than spacing (if $\lambda/2 < d$, then $\sin\theta > 1$, which is impossible). This condition is a limit on how many orders of diffracted waves can be obtained from assumed crystal using an x-ray beam of a given wavelength. The crystal patterns, indicated in three dimensions and denoted $(h \ k \ l)$ are required to

describe the order of the diffracted waves or called “the Miller indices”, which are used in crystallography, denote the orientation of the reflecting sheets with respect to the unit cell and the path difference in units of wavelength between identical reflecting sheets.

The X-ray diffraction technique is normally carried out by an X-ray diffractometer. The essential components of X-ray diffractometer (Fultz and Howe, 2008) are:

- 1) A source of X-ray, usually a sealed X-ray tube
- 2) A goniometer, which provides precise mechanical motions of the tube, specimen and detector
- 3) An X-ray detector
- 4) Electronics for counting detector pulses in synchronization with the positions of the goniometer

There are four practical approaches for observing diffractions and making diffraction measurements: Debye-Scherrer Method, Laue Method, Rotating Crystal Method and θ - 2θ diffractometer Method. All are designed to ensure that Bragg's law is satisfied. The schematic diagram of θ - 2θ X-ray diffractometer used in this work (BRUKER X-ray diffractometer model D5005 equipped with Cu $K\alpha$ sealed tube, wave length 1.54 Å) is shown in Figures 3.3 and 3.4. The θ - 2θ Diffractometer is used for diffraction measurements of unfixed horizontal sample. For this purpose, sample will be rotated to θ and X-ray detector moved to 2θ . The diffraction angle followed on Bragg's Equation (2.1). The one-side weight of the tube stand is compensated by a counter weight. Both tube stand and counter weigh are fixed to the outer ring.

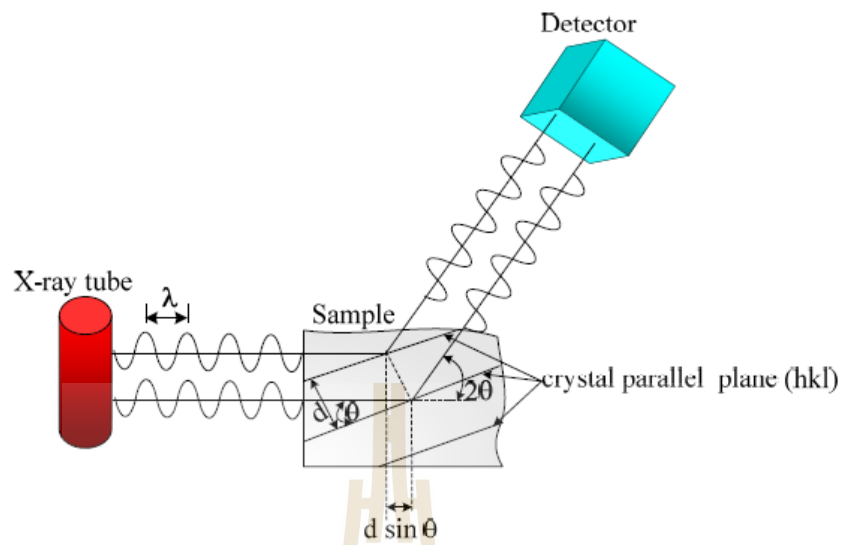


Figure 3.3 Schematic illustration of θ - 2θ X-ray diffraction experiment (Jutimoosik, 2010).

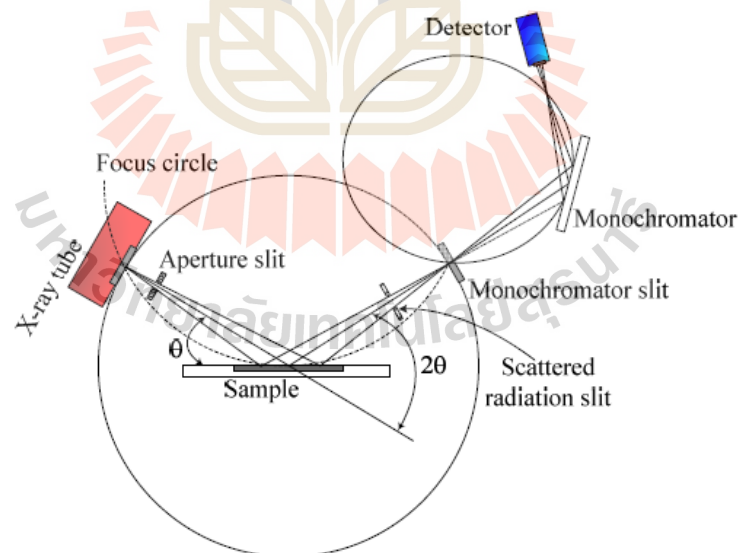
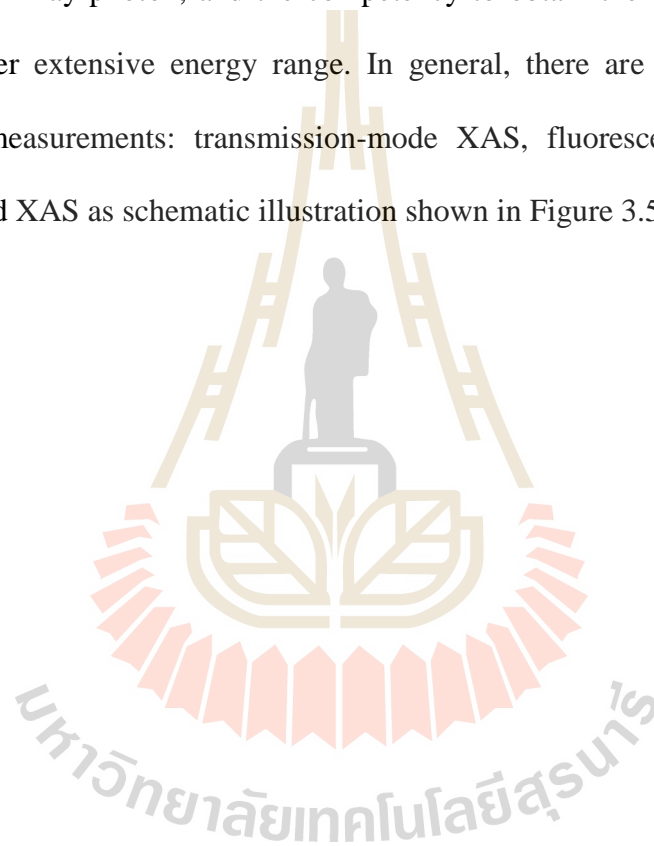


Figure 3.4 Schematic representation of X-ray diffractometer D5005 (Jutimoosik, 2010).

3.3 X-ray absorption spectroscopy setup

3.3.1 X-ray Absorption spectroscopy experimental setup Jeon *et al.*, (2010)

The X-ray absorption spectroscopy experiment is commonly accomplished at a synchrotron radiation source, due to high intensity and energy alterable competency of generated X-ray photon, and the competency to obtain the continuous absorption spectrum over extensive energy range. In general, there are three types of X-ray absorption measurements: transmission-mode XAS, fluorescence-mode XAS and electron-yield XAS as schematic illustration shown in Figure 3.5.



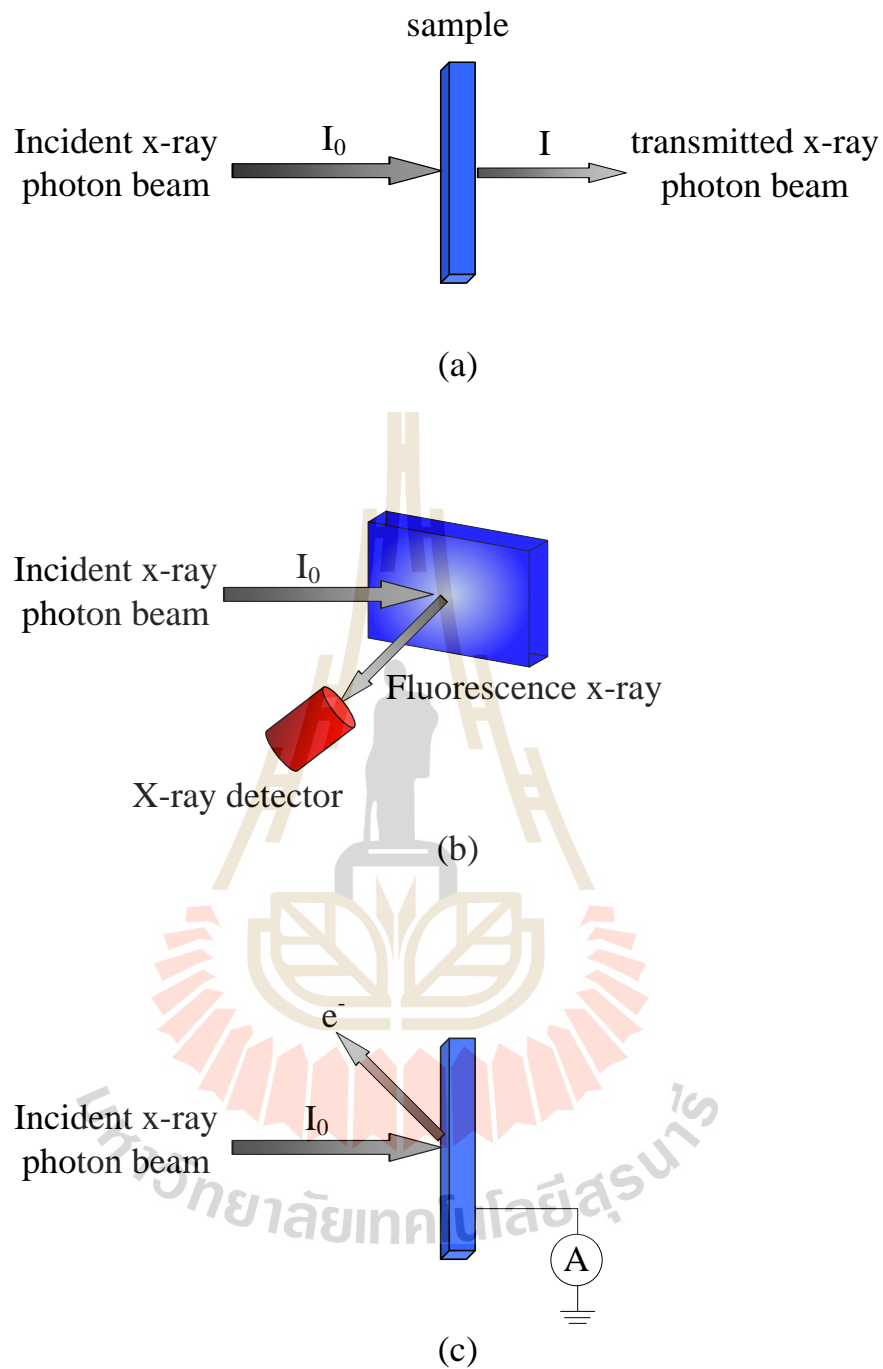


Figure 3.5 The three modes of XAS measurement (a) transmission mode, (b) fluorescence mode and (c) electron yield, adapted from (Kawai, 2000).

In transmission mode XAS, after the energy of X-ray photons being changed by X-ray double crystals monochromator, the intensities of incident X-ray photon beam

(I_0) and the transmitted X-ray photon beam (I) are measured by ionization chambers as shown in Figure 3.6. In this mode, we make sure the X-ray photon beam is well-aligned on the sample. The X-ray absorption can be extracted based on equation (2.24). The experimental set up of XAS experimental station at XAS beam line, Siam Photon Laboratory, SLRI is shown in Figure 3.7.

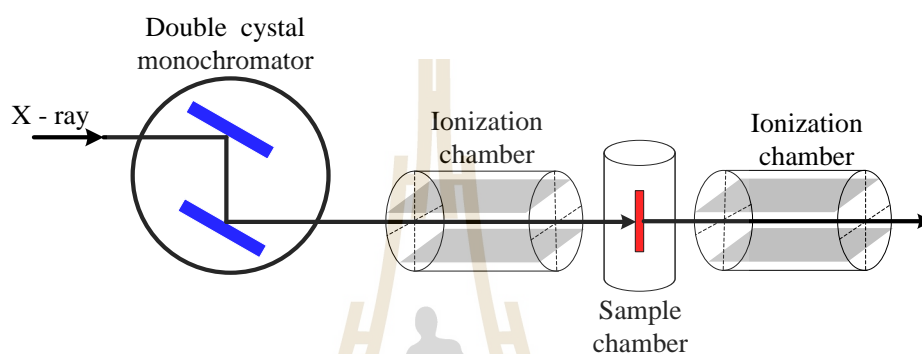


Figure 3.6 Schematic illustration of the experimental setup of transmission-mode X-ray absorption spectroscopy.



Figure 3.7 XAS experimental set up at the Siam Photon Laboratory, Synchrotron Light Research Institute with BL 5.

Other than the transmission mode, the fluorescence mode and the electron yield are also competent for the measurement of the absorption coefficient. In the X-ray absorption phenomena, where X-ray photon knock out an electron from the inner shell an electron from higher energy level will cascade down to fill in the hole and discharging radiation of energy, the discharged energy X-ray photon will be released as demonstrated in Figure 3.5(a) and the fluorescence X-ray can be detected. In addition, de-excitation can cause the Auger effect, where the electron reduce to lower energy state, a second electron can be excited to the continuum state and perhaps go out from the sample as shown in Figure 3.5(b), and then we can be detected it by using the electron-yield XAS detectors.

For fluorescence mode, we measure the intensities of incident X-ray photon beam and the fluorescence X-ray that are emitted following the X-ray absorption. Usually the fluorescence detector is placed at 90° to the incident X-ray photon beam in the horizontal plane, with the sample at an angle (usually 45°) with respect to the beam. Fluctuations in the number of elastically scattered X-ray are a significant source of noise in fluorescence XAS, so the position of the detector is selected to minimize the elastically scattered radiation by exploiting the polarization of the X-ray beam. In case of electron yield, we measure the electrons that are emitted from the surface of the sample. The relative short path length ($\approx 1000 \text{ \AA}$) makes the technique surface-sensitive, which can be beneficial if one is interested in near-surface phenomena. It also can be beneficial for avoiding “self absorption” effect that occurs in fluorescence mode. However, both modes are instantly equivalent to the absorption ability of the sample. Hence, the three techniques are alterable for the study of the structure of material using the absorption ability of the sample.

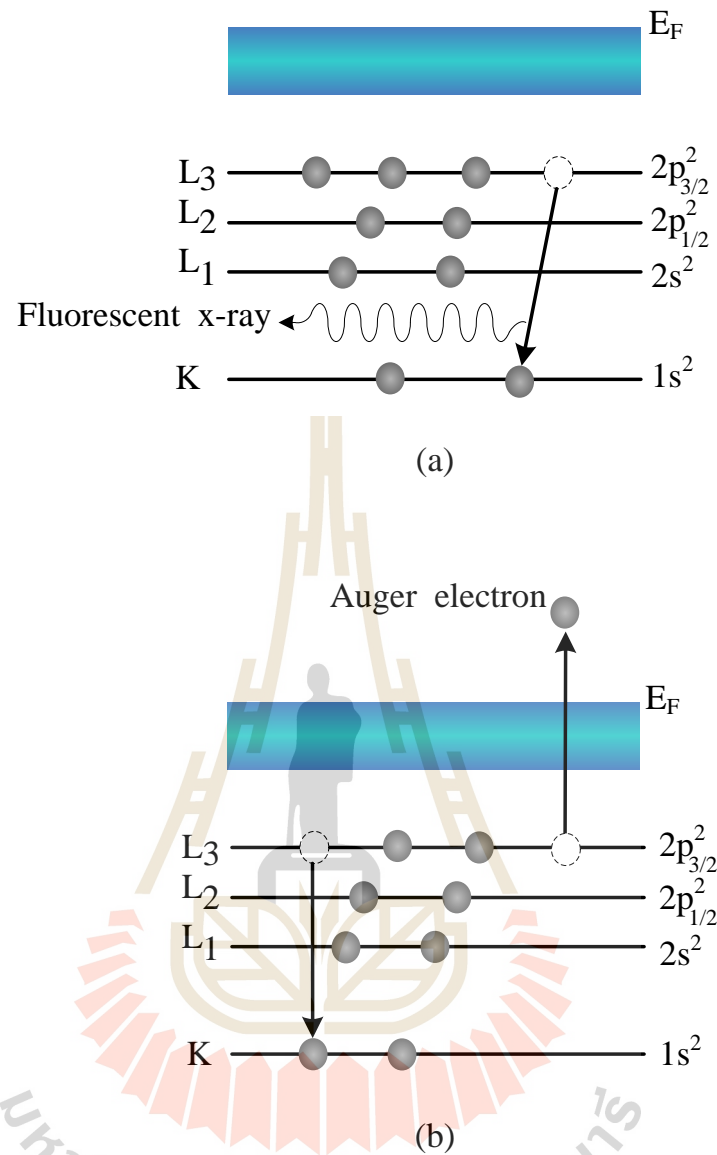


Figure 3.8 The excited state (a) X-ray fluorescence and (b) the Auger effect, adapted from (Koningsberger and Prins, 1988).

3.3.2 X-ray absorption spectrum calculation

In thesis, the principle theoretical calculations are performed based on FEFF 8.2 code. This code is developed to primarily calculate X-ray absorption for the FEFF (f_{eff}) project developed by the Department of Physics, University of Washington,

Seattle, USA. Apart from XAS spectra calculation, FEFF code can also calculate X-ray natural circular dichroism (XNCD), spin-dependent calculations of X-ray magnetic dichroism (XMCD), nonresonant X-ray emission (XES) and electronic structure including local densities of states (LDOS). FEFF code is written in ANSI FORTRAN 77 with principle investigator John J. Rehr and co-principle investigator Alexei L. Ankudinov.

FEFF is ab initio self-consistent real space multiple-scattering (RSMS) code for simultaneous calculations of X-ray absorption spectra and electronic structure. The input file “feff.inp” can be created directly from ATOMS code via “atoms.inp” as shown in Figure 3.9.

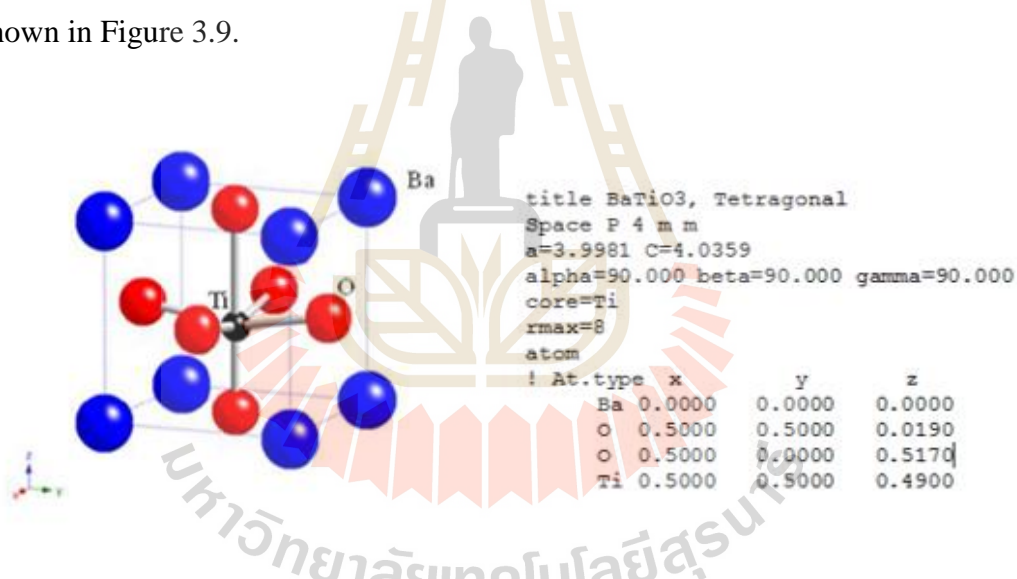


Figure 3.9 Detail of an *atoms.inp* input file to generate *feff.inp* for FEFF calculation.

```

TITLE  BaTiO3, Tetragonal

EDGE      K
S02      1.0

*
*      pot      xsph      fms      paths      genfmt      ff2chi
CONTROL  1      1      1      1      1      1
PRINT    1      0      0      0      0      0

*
*      r_scf    [ l_scf  n_scf  ca ]
SCF      4.18200  0      30    0.1

*
*      ixc    [ Vr  Vi ]
EXCHANGE 0      4    0.3

*EXAFS
*RPATH    8.36400

*
*      kmax    [ delta_k  delta_e ]
XANES    9.5    0.05  0.3
*
*      r_fms    [ l_fms ]
FMS      6.0    0
*
*
*RPATH    0.10000
*
*      emin    emax    resolution
*LDOS    -20    20    0.1

POTENTIALS
*
*      ipot    n [ label  l_scm  l_fms  stoichiometry ]
*      0      22  Ti    -1    -1    0
*      1      8   O    -1    -1    3
*      2     56  Ba    -1    -1    1
*      3     22  Ti    -1    -1    1

ATOMS
0.00000  0.00000  0.00000  0  Ti    0.00000
0.00000  0.00000 -1.90091  1  O    1.90091
-1.99905  0.00000  0.10897  1  O    2.00202
0.00000 -1.99905  0.10897  1  O    2.00202
1.99905  0.00000  0.10897  1  O    2.00202
0.00000  1.99905  0.10897  1  O    2.00202
0.00000  0.00000  2.13499  1  O    2.13499
1.99905  1.99905 -1.97759  2  Ba    3.45011

```

Figure 3.10 Detail of a “feff.inp” input file of MgO with Mg as center atom for FEFF calculation.

The suitable commands, parameter and atomic positions for FEFF-XAS spectrum calculations can be edited within the input file named “feff.inp”, which is shown in Figure 3.10. This file controlled with some details, for instance the generator

of input file and the number of atom which is contain in the cluster. The followed details describe about various card use to assign the steps of calculation. The type of atomic potentials and defined atomic symbols are presented in the next part, and eventually with the locations of the created atoms in the system where the location of center atom is placed at $(0, 0, 0)$ in (x, y, z) coordination.

3.4 Experimental Details

The global structure of $\text{Ba}(\text{Ti}_x\text{Ti}_{1-x})\text{O}_3$ was examined by X-ray diffraction (XRD) patterns which were scanned in 2θ range of 20° - 60° with 0.02° step and $\text{CuK}\alpha$ radiation was used. In addition, the local structure was examined by X-ray Absorption Spectroscopy (XAS) measurements which were conducted at room temperature at BL-5.2 of the Siam Photon Laboratory, Synchrotron Light Research Institute (SLRI), Thailand (electron energy of 1.2 GeV, beam current 120-80 mA). The synchrotron X-ray beam with energy step of 0.20 eV provides to excite the electrons in the Ti K -edge were measured by X-ray Absorption Near-Edge Structure (XANES) spectra for all compositions. The data were processed using the ATHENA program. The simulation was carried out using the FEFF8.2 program and qualitatively compared with XANES patterns obtained from the experiment. In addition, Extended X-ray Absorption Fine Structure (EXAFS) spectra were obtained for some compositions and processed using the ARTEMIS program (Chandarak *et al.*, 2012).

CHAPTER IV

RESULTS AND DISCUSSION

This chapter describes the experimental results on XRD and XAS measurements. The relationships between the two techniques are discussed.

4.1 X-ray diffraction (XRD)

The XRD patterns of BaTiO_3 and $\text{Ba}(\text{Fe}_x\text{Ti}_{1-x})\text{O}_3$ are shown in Figure 4.1 and Figure 4.2, respectively. It is seen that the global crystal structure, as determined by XRD, changes from tetragonal to hexagonal perovskite phases with increasing sintering temperature. The sample with BaTiO_3 shows the tetragonal perovskite phase, while the samples with Fe-BTO exhibit the XRD peaks with showing the mixing tetragonal and hexagonal phases. The standard tetragonal perovskite BaTiO_3 phase and hexagonal perovskite BaTiO_3 are also shown (matched with JCPDS file No.89-1428 and 82-1175, respectively).

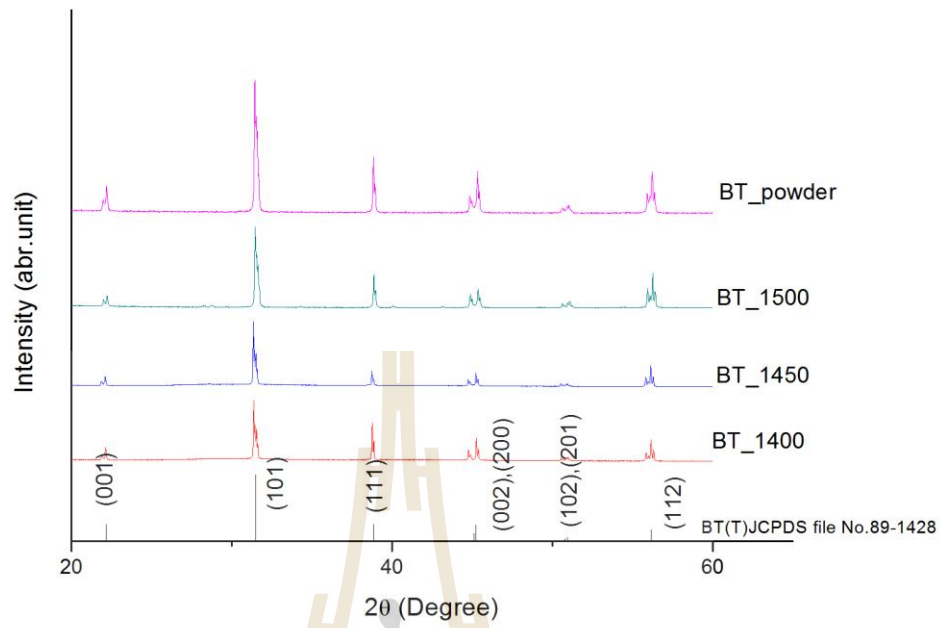


Figure 4.1 X-ray diffraction patterns of BaTiO₃.

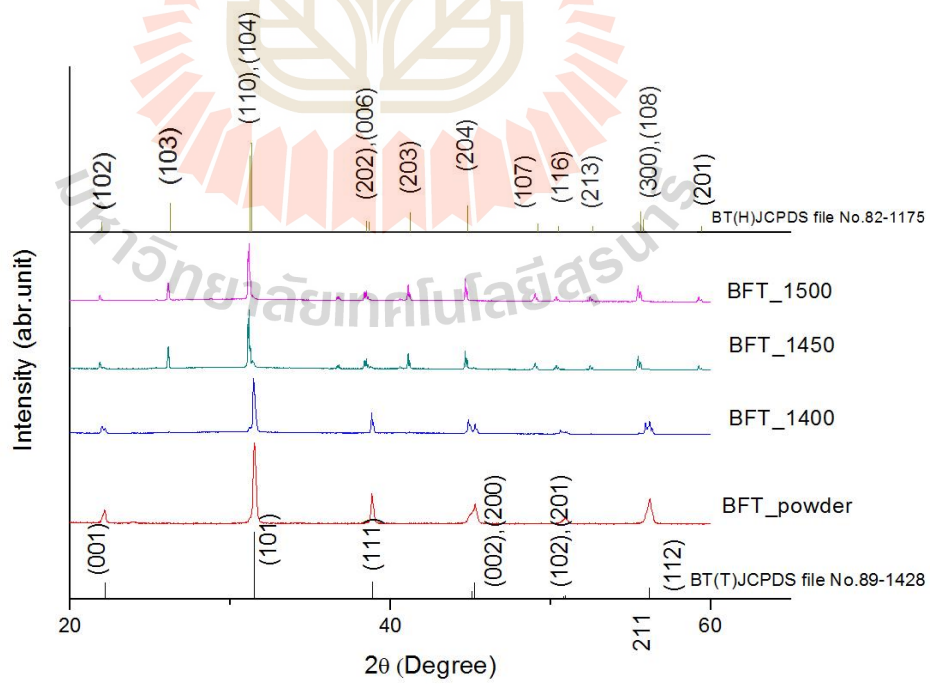


Figure 4.2 X-ray diffraction patterns of Ba(Fe_xTi_{1-x})O₃.

From the XRD results, the lattice parameters and the ratio of the combination phase could be obtained. By using the Rietveld refinement (Coelho Software Brisbane, Australia) analysis, the results are listed in Tables 4.1 and 4.2. Analysis of BaTiO₃ shows that the lattice parameters are similar, regardless of the sintering temperature and all samples show a tetragonal structure. The Fe-BTO samples show the mixing of tetragonal and hexagonal phases. Ratio of the hexagonal phase increases with the sintering temperature, and the lattice parameters increase with the sintering temperature, as well. This result corresponds to the previous studie (Mikulska *et al.*, 2014).

Table 4.1 The lattice parameters and the ratio of BaTiO₃.

Sample	Tetragonal			Hexagonal		
	a	c	%	a	c	%
BT_powder	3.9981	4.0359	100	-	-	-
BT_1400	3.9979	4.0388	100	-	-	-
BT_1450	3.9979	4.039	100	-	-	-
BT_1500	3.997	4.0221	100	-	-	-

Table 4.2 The lattice parameters and the ratio of $\text{BaFe}_{0.01}\text{Ti}_{0.99}\text{O}_3$.

Sample	Tetragonal			Hexagonal		
	a	c	%	a	c	%
BFT_powder	4.0044	4.0266	99.26	5.6565	13.888	0.74
BFT_1400	4.0008	4.035	95.982	5.7168	13.8883	4.018
BFT_1450	4.0409	4.0434	71.247	5.729	13.9834	28.726
BFT_1500	4.0474	4.0482	61.75	5.7322	13.9927	38.24

4.2 XANES results

4.2.1 Identification of Fe site in BaTiO_3

Generally, XANES measures the excitation of electrons K -levels to unoccupied bound states and is thus used to obtain information about the local arrangement of atoms around the absorbing atoms and the density of states of unoccupied states.

XANES spectra of Fe K -edge in Fe on Ti site in BaTiO_3 ($\text{Ba}(\text{Ti},\text{Fe})\text{O}_3$), Fe on Ba site in BaTiO_3 ($(\text{Ba},\text{Fe})\text{TiO}_3$) were obtained using the FEFF8.2 codes, following models in Figure 4.3. The FEFF codes is using a full multiple scattering approach based on ab initio overlapping muffin-tin potentials. The results show that the measured XANES is clearly consistent with the calculation of Fe on Ti site, and inconsistent with Fe at other lattice locations, as shown in Figure 4.4.

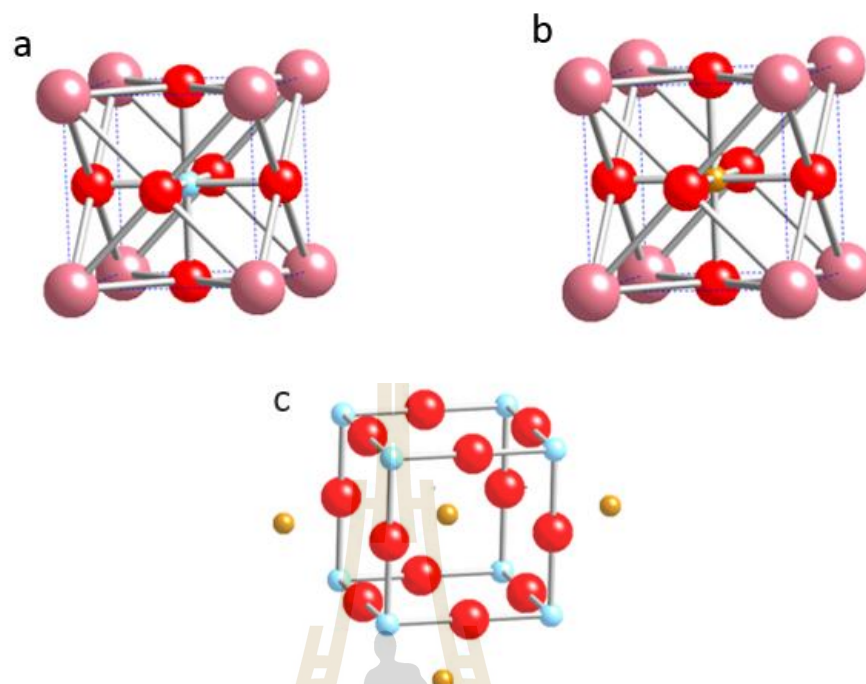


Figure 4.3 Model crystals structure of BaTiO₃. b–c Schematic illustrations of Fe on Ti site, Fe on Ba site, respectively.

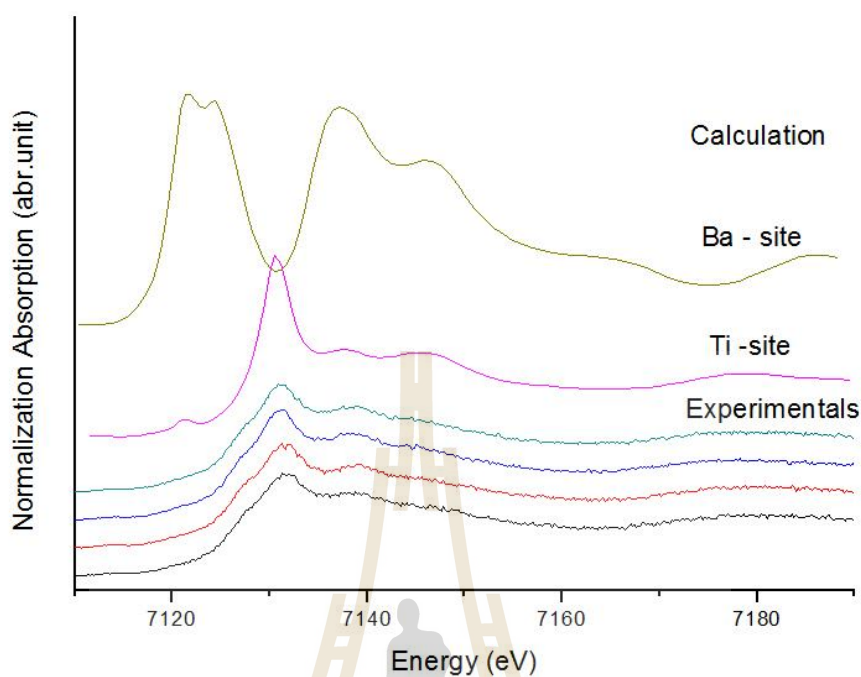


Figure 4.4 Fe K-edge XANES spectra of $\text{BaTi}_{0.99}\text{Fe}_{0.01}\text{O}_3$ and calculation of Fe site for Fe on Ti site (Fe_{Ti} -pink line), Fe on Ba site (Fe_{Ba} -gold line).

The measured XANES spectra for all samples were compared to those of standards: Fe foil, FeO and Fe_2O_3 , as shown in Figure 4.5. It was found that the absorption edges of Fe K-edge XANES spectrum for Fe_2O_3 are corresponding to those of Fe-doped BT samples. This agreement assures that doped Fe atoms in samples are 3^+ as same as Fe in Fe_2O_3 .

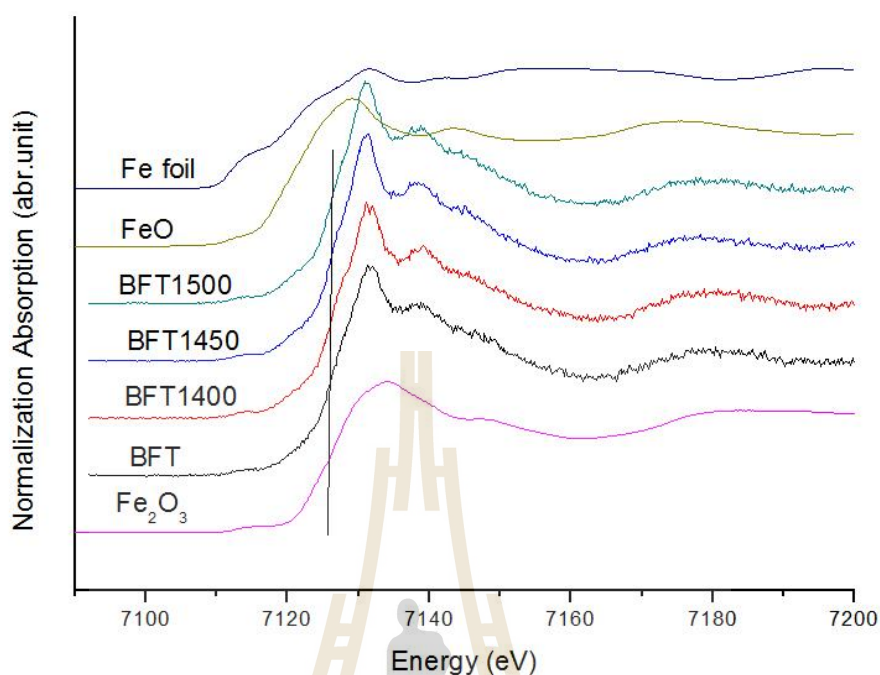


Figure 4.5 Normalized Fe K-edge XANES spectra measured on the Fe-BTO samples and reference compounds (Fe_2O_3 , FeO, and Fe foil) with known Fe valance state.

4.2.2 XANES studies of Ti K pre-edge

Generally, XANES measures the excitation of core electrons to unoccupied bound states and is thus used to obtain information about the local arrangement of atoms around the absorbing atoms and the density of states of unoccupied states⁵. According to the molecular orbital theory and valence band theory, 3d levels of the octahedral complex split into t_{2g} and e_g level. The integrated intensity of pre-edge is associated with probability of electrons 1s to t_{2g} and e_g level. However, transition of electrons from 1s to 3d levels are forbidden but, if Ti atoms is off center, it will be effect to 3d levels spiting lager until e_g levels overlap 4s levels and electrons 1s can

be occupied on eg levels more. Therefore, the integrated intensity of Ti K pre-edge, which is associated with both the quadrupole and the dipole $1s \rightarrow 3d$ transition of Ti, reflects the $3d-4p$ hybridization for Ti and I_A is directly proportional to the displacements of Ti off-center of oxygen octahedra and is indirectly proportional to the lattice constants (Vedrinskii *et al.*, 1998; Levin *et al.*, 2011). The integrated intensity of peak B is associated with both the quadrupole and the dipole $1s \rightarrow 3d$ transition in molecular orbital related the local Fe/Ti ratio around the absorbing Ti.

The normalized Ti K pre-edge XANES spectra of $\text{BaFe}_{0.01}\text{Ti}_{0.99}\text{O}_3$ are shown in Figure 4.6. According to Equation (3.3), we adopted this value as a reference for calculating local Ti off-centering from the pre-edge peak intensities in the solid solution samples.

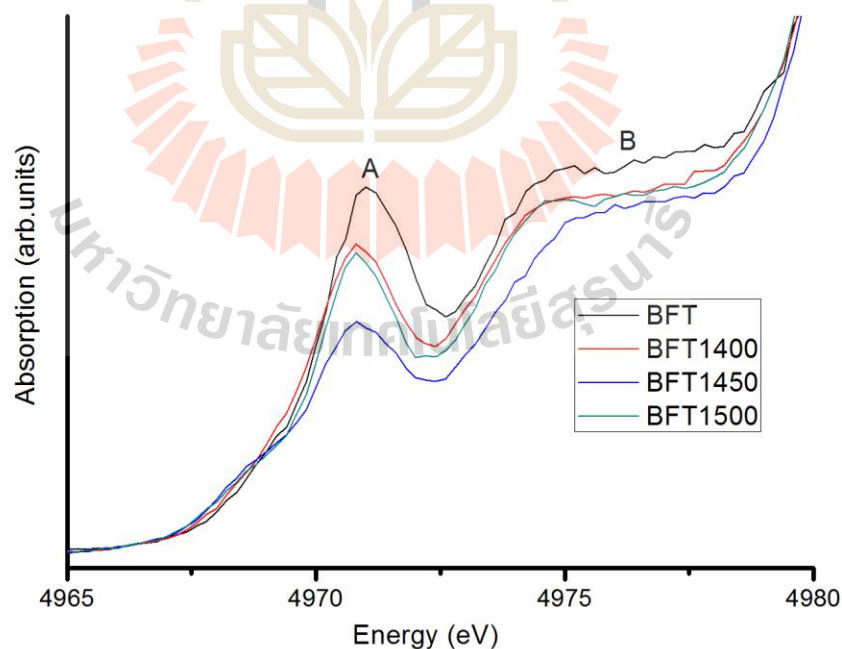


Figure 4.6 Normalized X-ray absorption Ti K pre-edge spectra of Fe-BTO.

4.2.3 XANES studies of phase transition.

The normalized Ti *K*-edge XANES spectra of Fe-BTO are shown in Figure 4.7. While XANES spectra only show little difference in features for compositions with Fe-BTO, the spectra exhibit a clear change in features with the shift in the peak C to the left-hand side; an indication of the change in local structure around Ti absorbing atom. This means that Ti atoms should locally move toward central of oxygen octahedra. However, this shift in the location of Ti cannot be observed by XRD. The XANES spectrum can be simulated using the unoccupied electronic states of the system, as described below.

The X-ray absorbance $\mu(E)$ is given by Fermi's golden rule. Simulated XANES spectra of Ti *K*-edge in Fe-deficient $\text{Ba}(\text{Ti},\text{Fe})\text{O}_3$ and Fe-enriched $\text{Ba}(\text{Ti},\text{Fe})\text{O}_3$ were obtained using the FEFF8.2 code. The FEFF code employs a full multiple scattering approach based on *ab initio* overlapping muffin-tin potentials. The muffin-tin potentials used in FEFF codes are self-consistent calculations with Hedin-Lundqvist exchange-correlation function (Hedin and Lundqvist, 1970; Rehr and Albers, 2000). It should be noted here first that, to simulate the XANES spectra of Ti, the structural model with Ti-off center in tetragonal perovskite structure ($\alpha=\beta=\gamma=90$) and hexagonal structural model ($\alpha=\beta=90,\gamma=120$). The simulation of the XANES spectra of the BFT phase was subsequently carried out to investigate the feature around Ti absorbing atoms in BFT solid solution with the simulated and experimental results compared in Figure 4.8. However, the simulated spectral features from the tetragonal structure $\text{Ba}(\text{Ti},\text{Fe})\text{O}_3$ is in good agreement with the experimental XANES spectra. This agreement between the experimental and simulated spectra indicates that for $\text{Ba}(\text{Ti},\text{Fe})\text{O}_3$ compositions with low Fe content the local structure shows a

mixture of tetragonal and hexagonal structure, even though the XRD results exhibit the (global) tetragonal perovskite structure. The structure is close to the tetragonal perovskite, as observed in both XAS and XRD measurements.

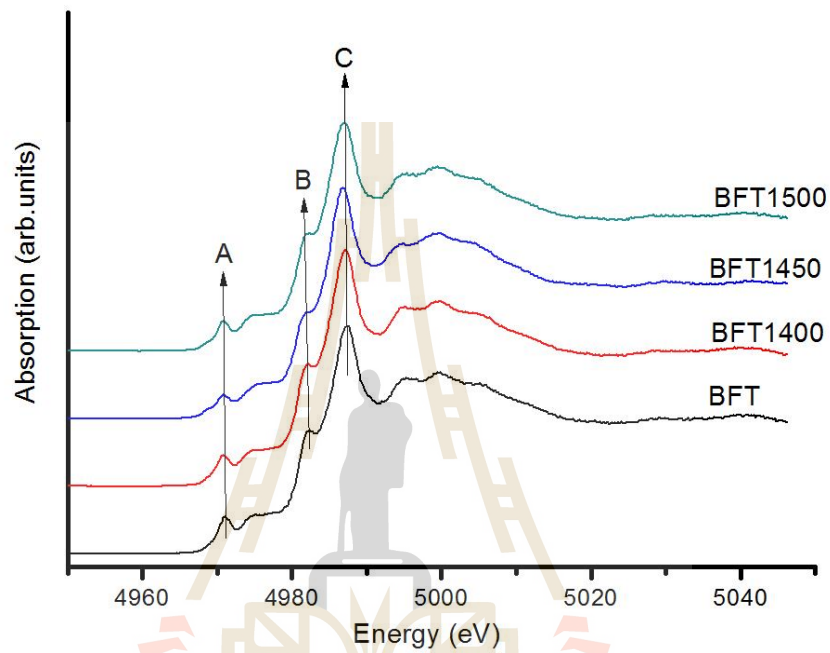


Figure 4.7 Normalized X-ray absorption Ti K-edge spectra of Ba(Fe_xTi_{1-x})O₃.

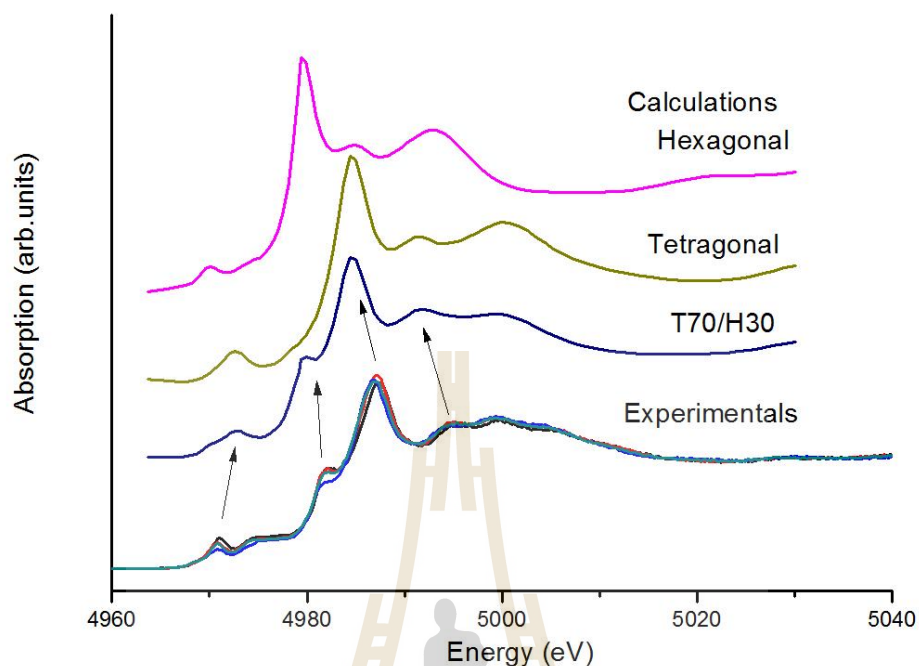


Figure 4.8 Comparison of Normalized X-ray absorption Ti K-edge spectra of $\text{Ba}(\text{Fe}_x\text{Ti}_{1-x})\text{O}_3$ with simulated features of Ti K-edge XANES spectra of $\text{Ba}(\text{Fe},\text{Ti})\text{O}_3$ tetragonal (pinkline) and hexagonal (gold line).

4.3 EXAFS results

To process and enhance the EXAFS with the high k region, the plot $k^2X(k)$ is considered and windowed using a Hanning window $W(k)$. The EXAFS spectra were processed and information on local structure of Fe atom is obtained via fitting with perovskite models of $\text{Ba}(\text{Ti},\text{Fe})\text{O}_3$ in ARTEMIS program.

In this work, the Fe K -edge EXAFS spectra did not show clearly the phase transition. Therefore, the Fe K -edge EXAFS spectra can be changed to the normalized experimental EXAFS signal (χ) in function k , as shown in Figure 4.10. For BFT_1400- BFT_1500 samples, the phase transition of tetragonal and hexagonal is

likely seen from the XANES spectra. A comparison between the simulated EXAFS model and experimental EXAFS is shown in Figure 4.11. It should be mentioned that the combination of both tetragonal and hexagonal structures results in a better fitting with the experimental results in Figure 4.10.

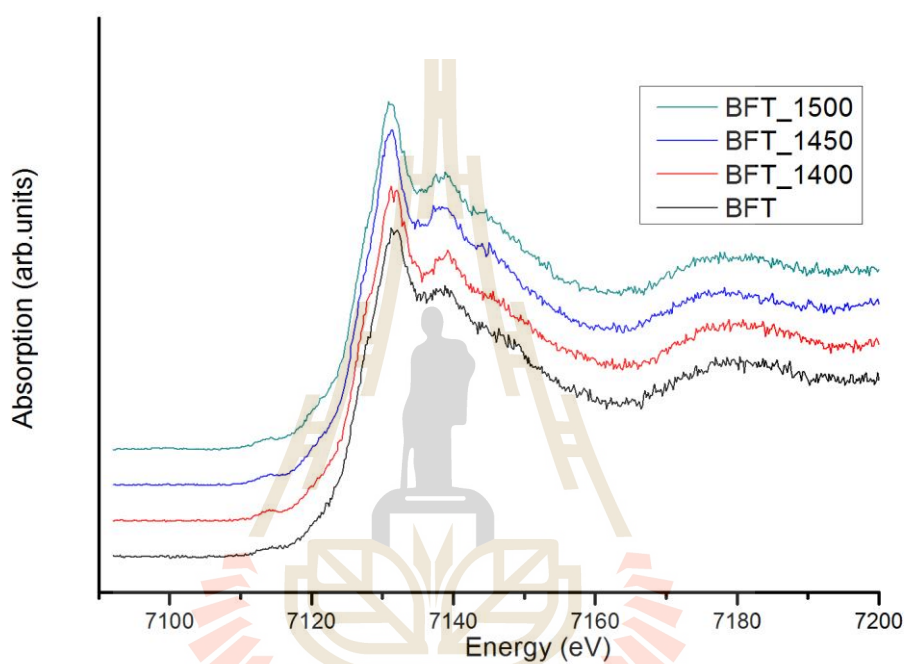


Figure 4.9 The Normalized Fe K-edge EXAFS spectra of Ba(Ti,Fe)O₃.

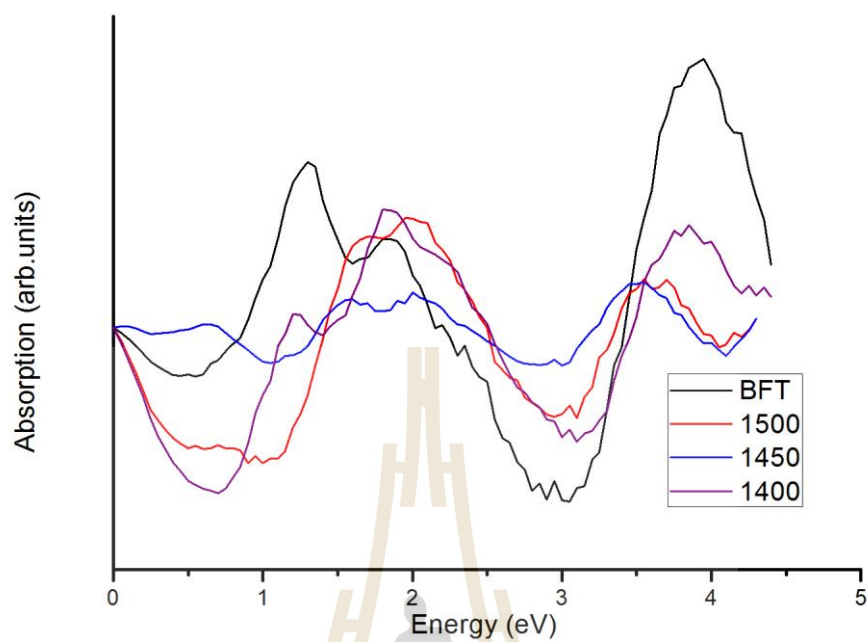


Figure 4.10 The EXAFS Fourier transform in k-space of Ba(Ti,Fe)O₃.

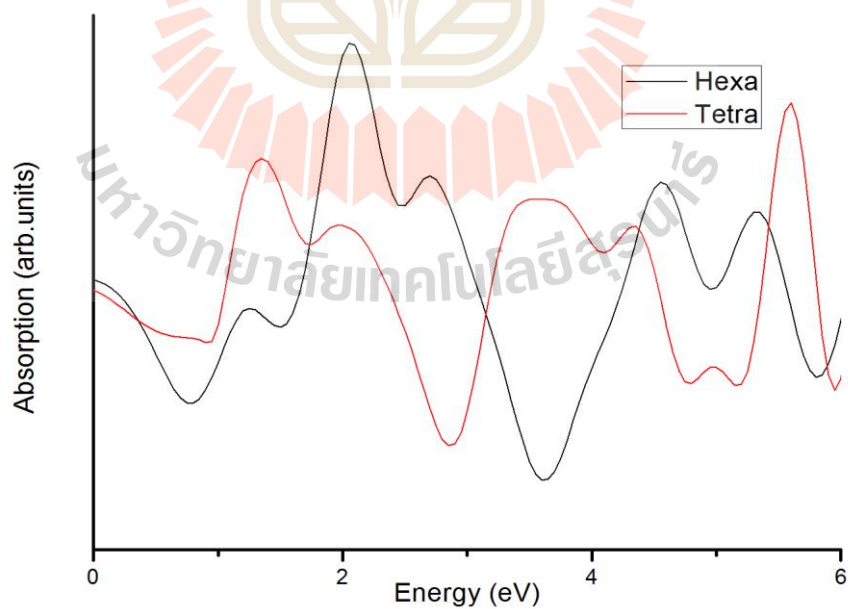
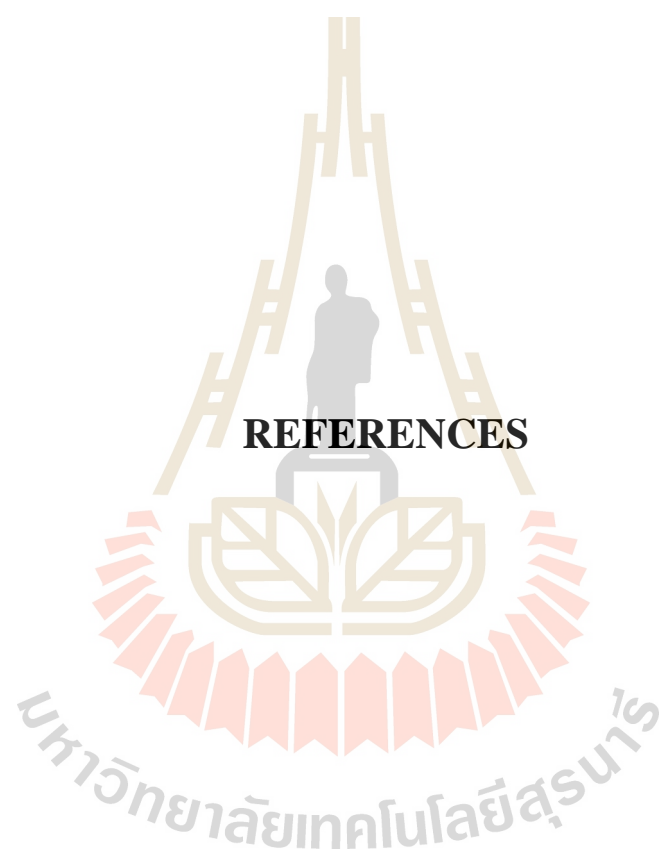


Figure 4.11 The simulation EXAFS models in k-space of Ba(Ti,Fe)O₃.

CHAPTER V

CONCLUSIONS

In this work, the global and local structural information of Fe-doped BaTiO₃ materials was examined by X-ray Diffraction (XRD) and Synchrotron X-ray Absorption Spectroscopy (XAS) techniques, respectively. XAS technique was employed to investigate the local structure of the BaTiO₃-based materials. The synchrotron XANES and EXAFS measurements were performed at the X-ray absorption spectroscopy beamline BL-5.2 of the Synchrotron Light Research Institute (SLRI, Thailand) for understanding the phase transition of perovskite structure in Fe-doped BaTiO₃ (Fe-BTO) materials. The XRD results showed the mixed global structures of tetragonal and hexagonal phases with increasing sintering temperature. Both Fe dopant and sintering temperature are seen to cause the changes of the crystalline phase in BaTiO₃. In addition, the experimental and simulated XAS results represent the combination of tetragonal and hexagonal phases. It is also noted that Fe-dopants occupy the Ti-site in BaTiO₃ lattice, as confirmed by both experimental and simulated XANES results.



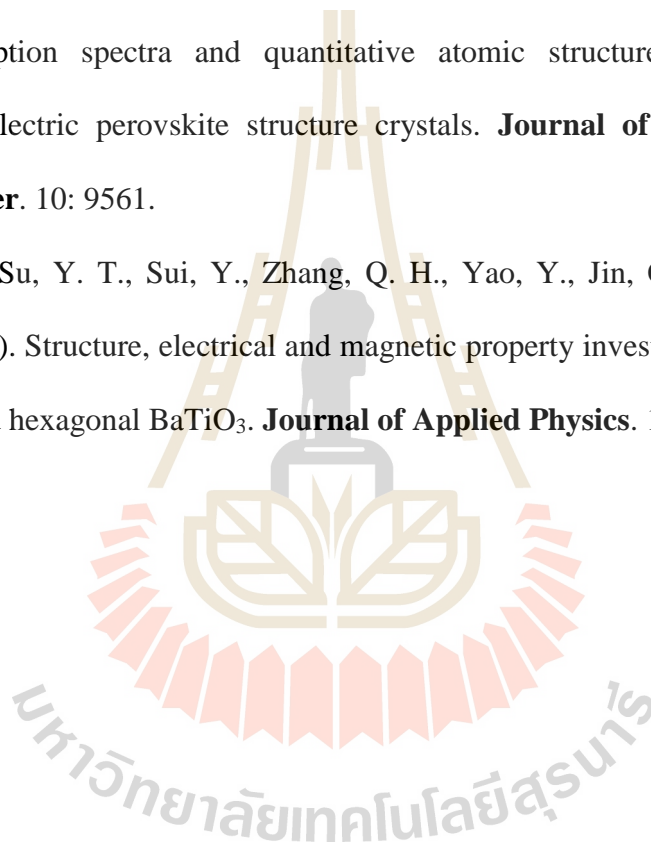
REFERENCES

REFERENCES

- Ankudinov, A. L., Ravel, B., Rehr, J. J., and Conradson, S. D. (1998). Real-space multiple-scattering calculation and interpretation of x-ray-absorption near-edge structure. **Physics Review B**. 58: 7565.
- Bootchanont, A., Jutimoosik, J., Chandarak, S., Unruan, M., Kidkhunthod, P., Klysubun, W., Rujirawat, S., Yimnirun, R., Guo, R., and Bhalla, A. (2014). Synchrotron X-ray absorption spectroscopy study of local structure transformation behavior in perovskite Ba(Ti,Zr)O₃ system. **Journal of Alloys and Compounds**. 616: 430–435.
- Chandarak, S., Jutimoosik, J., Bootchanont, A., Unruan, M., Jantaratang, P., Priya, S., Srilomsak, S., Rujirawat, S., and Yimnirun, R. (2012). Local Structure of Magnetolectric BiFeO₃-BaTiO₃ Ceramics Probed by Synchrotron X-Ray Absorption Spectroscopy. **Journal of Superconductivity and Novel Magnetism**. 26: 455.
- Fultz, B., and Howe, J. M. (2008). **Transmission electron microscopy and diffractometry of materials** (3rd ed.). New York: Springer.
- Gene H. Haertling (1999). Ferroelectric Ceramics: History and Technology. **Journal of the American Ceramic Society**. 82 (4): 797–818.
- Iuliia Mikulska, Matjaz Valant, Iztok Arcon, and Darja Lisjak. (2015). X-ray Absorption Spectroscopy Studies of the Room-Temperature Ferromagnetic

- Fe-Doped 6H-BaTiO₃. **Journal of the American Ceramic Society**. 98: 1156–1161. Jeon, J.-S., Kim, B.-H., Park, C.-I., Seo, S.-Y., Kwak, C., Kim, S.-H., and Han, S.-W. (2010). In-situ X-ray Absorption Fine Structure Study of TiO₂ Nanoparticles under Ultraviolet Light. **Japanese Journal Applied Physics**. 49.
- Jutimoosik, J. (2010). **Local Structure of Magnesium Zinc Oxide Nanocrystals**. M.S. thesis, Suranaree University of Technology, Nakhon Ratchasima.
- Kawai, J. (2000). **Absorption techniques in x-ray spectrometry, Encyclopedia of analytical chemistry**. New York: Wiley.
- Khamkongkao, A. (2013). **Electrical and Magnetic Properties of Cobalt Ferrite and Cobalt Ferrite-Barium Titanate Nanocomposites**. Ph.D.Thesis Khon Khen University, Khon Khen.
- Koningsberger, D. C., and Prins, R. (1998). **X-ray Absorption: Principles, Applications, Techniques of EXAFS, SEXAFS and XANES**. New York: Wiley.
- Maiti, T., Guo, R., and Bhalla, A. S. (2008). Structure-Property Phase Diagram of BaZr_xTi_{1-x}O₃ System. **Journal of the American Ceramic Society**. 91: 1769.
- Ravel, B. D. (1997). **Ferroelectric Phase Transition in Oxide Perovskites Studied by XAFS**. University of Washington, Washington.
- Shanthakumar. P. (2008). **X-ray Study of Two Complex Oxides, each Having Octahedral oxygen co-ordination of transition metals**. University of Connecticut, Connecticut.

- Thompson, A. C., Attwood, D. T., Gullikson, E. M., Howells, M. R., Jeffrey B. Kortright, Robinson, A. L., Underwood, J. H., Kim, K.-J., Kirz, J., Lindau, I., Pianetta, P., Winick, H., Williams, G. P., and Scofield, J. H. (2001). **X-RAY DATA BOOKLET**. Berkeley: Lawrence Berkeley Laboratory.
- Vedrinskii, R. V., Kraizman, V. L., Novakovich, A. A., Demekhin, P. V., and Urazhdin, S. V. (1998). Pre-edge fine structure of the 3d atom K X-ray absorption spectra and quantitative atomic structure determinations for ferroelectric perovskite structure crystals. **Journal of Physics Condensed Matter**. 10: 9561.
- Wei, X. K., Su, Y. T., Sui, Y., Zhang, Q. H., Yao, Y., Jin, C. Q., and Yu, R. C. (2011). Structure, electrical and magnetic property investigations on dense Fe-doped hexagonal BaTiO₃. **Journal of Applied Physics**. 110: 114112.



CURRICULUM VITAE

Name Miss Suntaree Tongsaeng

Date of Birth 25 March 1991

Place of Birth Udon Thani, Thailand

Education

2009-2013 Bachelor of Science in Physics,
Khon Kean University, Khon Kean, Thailand

2013-Present Currently enrolling in Master's degree majoring in Applied
Physics, School of Physics, Institute of Science, Suranaree
University of Technology, Nakhon Ratchasima, Thailand

มหาวิทยาลัยเทคโนโลยีสุรนารี